

## QCD matter in extreme environments

K Fukushima

Department of Physics, Keio University,  
3-14-1 Hiyoshi, Kohoku-ku, Yokohama-shi, Kanagawa 223-8522, Japan

**Abstract.** We review various theoretical approaches to the states of QCD matter out of quarks and gluons in extreme environments such as the high-temperature states at zero and finite baryon density and the dimensionally reduced state under an intense magnetic field. The topics at high temperature include the Polyakov loop and the 't Hooft loop in the perturbative regime, the Polyakov loop behaviour and the phase transition in some of non-perturbative methods; the strong-coupling expansion, the large- $N_c$  limit and the holographic QCD models. These analyses are extended to hot and dense matter with a finite baryon chemical potential. We point out that the difficulty in the finite-density problem has similarity to that under a strong magnetic field. We make a brief summary of results related to the topological contents probed by the magnetic field and the Chiral Magnetic Effect. We also address the close connection to the (1+1) dimensional system.

Submitted to: *J. Phys. G: Nucl. Part. Phys.*

## 1. Introduction

The inside of heavy nuclei is already a very interesting and peculiar environment. It is known that the density of nucleons, i.e. the baryon density, takes an almost constant value,  $\rho_0 \simeq 0.17$  nucleon/fm<sup>3</sup>, in the central region of nuclei independently of the atomic number  $A$  for large enough  $A$ . In terms of our daily units this normal nuclear density is as huge as  $\sim 10^{12}$  g/cm<sup>3</sup>. When two heavy nuclei (positively charged ions) collide at almost the speed of light, an enormous energy is crammed in a volume of size of heavy nuclei with the (transverse) radius  $r_A \sim 1.2A^{1/3}$  fm. In this way the relativistic heavy-ion collision experiment provides us with an ideal opportunity to examine the state of matter under extreme environments as have ever existed in the Universe.

The collision energy is finally released into a form of the energy conveyed by produced particles. Measuring the momentum distribution of those particles, the initial energy density can be deduced, which is summed up as the Bjorken formula (though it looks slightly different from the original form [1]),

$$\epsilon_0 = \frac{\langle m_\perp \rangle}{\tau_0 \pi r_A^2} \cdot \frac{dN}{dy} , \quad (1)$$

where  $\tau = \sqrt{t^2 - z^2}$  and  $y = \frac{1}{2} \ln[(t+z)/(t-z)]$  are the proper time and the coordinate rapidity, respectively. Each produced particle has energy  $m_{\perp} = \sqrt{p_{\perp}^2 + m^2}$  with the transverse momentum  $p_{\perp}$ . The number of particle is represented by  $N$ . The energy density is then given by the energy of particle  $\langle m_{\perp} \rangle dN$  divided by the initial volume  $\tau_0 \pi r_A^2 dy$ , where  $\tau_0$  denotes the initial time when particles are produced.

Once the thermal equilibrium is reached and deconfined gluons and  $N_f$ -flavour quarks – the fundamental objects in Quantum Chromodynamics (QCD) – are assumed to be massless particles, the energy density  $\epsilon$  is translated into the temperature  $T$  through the Stefan-Boltzmann law;  $\epsilon = (\pi^2/30) n(T) T^4$  where  $n(T) = 16$  (gluons) +  $10.5 N_f$  (quarks) is the effective number of physical degrees of freedom. The Monte-Carlo simulation of finite- $T$  QCD discretized on the lattice (see references [2, 3] for recent advances) has identified the pseudo-critical temperature as  $T_c \simeq (150\text{--}160)$  MeV. This  $T_c$  value corresponds to the critical energy density,  $\epsilon_c \simeq (0.8\text{--}1.0)$  GeV/fm<sup>3</sup>, beyond which the state of matter should be composed of gluons and quarks, namely, a quark-gluon plasma (QGP) is realised. We note that the energy density at normal nuclear density  $\rho_0$  is  $m_N \rho_0 \simeq 0.16$  GeV/fm<sup>3</sup> with the nucleon mass  $m_N = 0.94$  GeV used, that is about one fifth smaller than  $\epsilon_c$ .

In the facilities called the Alternating Gradient Synchrotron (AGS) at BNL and the Super Proton Synchrotron (SPS) at CERN the heavy-ion (Au-Au at AGS and Pb-Pb at SPS) experiments with a fixed target had been conducted since 1986. There, at the collision energy (per nucleon-nucleon)  $\sqrt{s_{NN}} = 17.2$  GeV at SPS, some theoretical study [4] led to an estimate  $\epsilon_0 = (1.2\text{--}2.6)$  GeV/fm<sup>3</sup> (at  $\tau_0 = 0.8$  fm). This initial energy density exceeds the critical value, so that the state of matter created at SPS could be a QGP possibly. It has become evident in the Relativistic Heavy Ion Collider (RHIC) at BNL, which has been in operation since 2000, that the collision energy  $\sqrt{s_{NN}} = 200$  GeV is high enough to form the QGP with the initial energy density  $\epsilon_0 = (12\text{--}20)$  GeV/fm<sup>3</sup> (at  $\tau_0 = 0.6$  fm).

The experimental activities are still continued; there are two major directions as the future plan; one is the direction towards higher  $T$  at larger collision energies, while the other is the direction towards higher baryon density at smaller energies. The former is already ongoing since 2010 in the Large Hadron Collider (LHC) at CERN, where the experimental data from the Pb-Pb collision at  $\sqrt{s_{NN}} = 2.76$  TeV are significantly improving the quality of analysis. It is said that the QGP physics has been promoted from the “discovery stage” to the “precision science” studies. The latter direction, i.e. the extrapolation to higher baryon density regions and the experimental survey over the whole QCD phase diagram, is also underway. The beam-energy scan program at RHIC aims to give a detailed portrait of the phase structure of QCD matter, especially to locate a special point of the exact second-order phase transition called the QCD critical point [5, 6, 7, 8, 9], which would serve as a landmark. The RHIC energy scan will be complemented by future experiments planned in the Facility for Antiproton and Ion Research (FAIR) at GSI, the Nuclotron-based Ion Collider Facility (NICA) at JINR and perhaps the Japan Proton Accelerator Research Complex (JPARC) at JAERI.

This review is a self-contained summary of some selected approaches in theory to the physical properties of QCD matter under extreme environments such as the high temperature in section 2 and the finite baryon density in section 3. It is, however, practically impossible to cover all the topics related to finite temperature/density QCD here. We shall specifically focus on the deconfinement physics and the dynamics of the order parameter called the Polyakov loop. As for the phase structure associated with chiral-symmetry breaking and restoration, the interested readers may consult my reviews [10, 11] and other reviews [12, 13, 14, 15, 16, 17, 18] and references therein. In particular my previous reviews [10, 11] include a pedagogical introduction to more generic physics of hot and dense QCD and subjects related to chiral-symmetry breaking, but not much about deconfinement physics. Hence, this present review is complementary to [10, 11] in respect to deconfinement physics and the Polyakov loop dynamics.

The last half of this review is devoted to a new physics possibility in a strong magnetic field  $\mathbf{B}$  produced by non-central collisions. The strength of this produced  $\mathbf{B}$  surpasses the surface magnetic fields on the neutron star by orders of the magnitude. The presence of the magnetic background which is as strong as the QCD energy scale  $\Lambda_{\text{QCD}} \sim 200$  MeV may well affect experimental observables considerably. A systematic procedure to resum relevant diagrams important at strong  $\mathbf{B}$  has not been better established on the practical level than the finite temperature/density field theory. Therefore our discussions in section 4 shall be not conclusive enough but aim to be comprehensive over various aspects of the phenomenon known as the Chiral Magnetic Effect.

## 2. High-temperature State of QCD

At sufficiently high temperature we can make use of the perturbative expansion in terms of the strong coupling constant,  $g$ , since the renormalisation of the UV divergences and the independence of the renormalisation point make  $g$  or  $\alpha_s = g^2/4\pi$  run as a function of the momentum scale  $\mu$ ; at the one-loop order,

$$\alpha_s(\mu^2) = \frac{\alpha_s(\mu_0^2)}{1 + \beta_0 \alpha_s(\mu_0^2) \ln(\mu^2/\mu_0^2)}, \quad (2)$$

where  $\beta_0 = (11 - \frac{2}{3}N_f)/4\pi$ . For the reference scale  $\mu_0$ , it is a conventional choice to set  $\mu_0$  as the  $Z_0$  boson mass,  $M_Z = 91.2$  GeV and the world average at present is  $\alpha_s(M_Z^2) = 0.1184(7)$  [19]. It is natural from equation (2) to consider that the strong coupling constant gets smaller at higher temperature where the typical momentum scale among thermally interacting particles is characterised by the temperature  $T$ . One could therefore take  $\mu \propto T$  but cannot precisely fix the proportionality coefficient because it is not clear which renormalisation condition is the most efficient to resum the higher-order diagrams. The conventional prescription is to take  $\mu = 2\pi T$  and vary  $\mu$  to check the stability of the physical results [20] (see also [21] for a review).

While the perturbative QCD calculations are useful at high temperature, it is necessary to develop a non-perturbative method to go down towards  $T_c$ . In this section

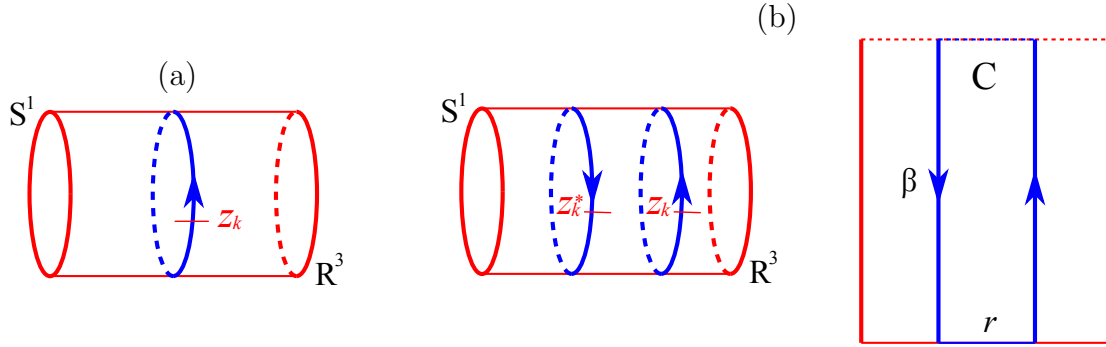


**Figure 1.** (a) Graphical representation of the Polyakov loop in Euclidean space-time. The centre transformation multiplies  $z_k$  on the Polyakov loop matrix. (b) Left: Polyakov loop correlator that is a counterpart of the closed Wilson loop. The correlator is centre invariant because  $z_k \cdot z_k^* = 1$ . Right: An opened-up figure whose temporal edges are contracted by the periodic boundary condition.

we first look over the perturbative results, and then, we will proceed to several non-perturbative approaches. As we have stated, in this review, we mostly address the pure gluonic sector and the deconfinement order parameter. We postpone the discussions on dynamical quark effects to section 3.

The conventional choice of the order parameter for quark deconfinement at finite temperature is the (traced) Polyakov loop [22, 23]. The Polyakov loop matrix and its traced quantity are denoted respectively as

$$L = \mathcal{P} \exp \left[ ig \int_0^\beta dx_4 A_4(\mathbf{x}, x_4) \right], \quad \Phi = \frac{1}{N_c} \langle \text{tr} L \rangle, \quad (3)$$

in the imaginary-time formalism of the finite-temperature field theory. Figure 1 (a) is a graphical representation on the manifold of  $\mathbb{S}^1 \times \mathbb{R}^3$ . The Polyakov loop expectation value,  $\Phi$ , can be interpreted as the partition function in the presence of a static-quark source. The logarithm of  $\Phi$  thus yields the single-quark free energy  $f_q$  as in standard thermodynamics;  $f_q = -T \ln \Phi$ . In the quark deconfined phase  $\Phi$  and  $f_q$  take a non-zero value, whereas  $\Phi \rightarrow 0$  and  $f_q \rightarrow \infty$  in the quark confined phase.

This behaviour of the Polyakov loop is understood from Wilson's standard criterion of confinement [24]. As seen in figure 1 (b) the Wilson loop on  $\mathbb{S}^1 \times \mathbb{R}^3$  amounts to the correlator of the Polyakov loop  $L$  and the anti-Polyakov loop  $L^\dagger$ . In the confined phase the Wilson loop shows the area law (in the absence of dynamical quarks) and the deconfinement phase results in the perimeter law, which can be interpreted in terms of the Polyakov loop as

#### Confined Phase

$$\langle W(C) \rangle \sim e^{-\sigma_w \Sigma(C)} \rightarrow \langle \text{tr} L^\dagger(r \rightarrow \infty) \text{tr} L(0) \rangle \rightarrow 0 \quad \rightarrow \Phi = 0 \quad (4)$$

#### Deconfined Phase

$$\langle W(C) \rangle \sim e^{-\sigma'_w L(C)} \rightarrow \langle \text{tr} L^\dagger(r \rightarrow \infty) \text{tr} L(0) \rangle \rightarrow (\text{const.}) \rightarrow \Phi \neq 0, \quad (5)$$

where  $\Sigma(C) = \beta r$  is the area enclosed by  $C$  and  $L(C)$  is the perimeter (see figure 1 (b)).

This criterion is related to the global symmetry of QCD that makes the Polyakov loop expectation value vanishing. To manifest this symmetry let us turn to the lattice approximation to equation (3), i.e.

$$L = \prod_{n_4=0}^{N_\tau-1} U_4(\mathbf{x}, x_4 = an_4). \quad (6)$$

Here  $U_4 = e^{-igaA_4}$  is the temporal link variable. (Note that in equation (6) the time product is from the left to the right with increasing time, while later time comes to the left in equation (3).) Then, under a general gauge transformation, the link variable changes as

$$U_\mu(x) \rightarrow V(x)U_\mu(x)V^\dagger(x + a\hat{\mu}). \quad (7)$$

Therefore, the following transformation belongs to a subgroup of the gauge transformation,

$$U_4(\mathbf{x}, x_4 = a(N_\tau - 1)) \rightarrow z_k U_4(\mathbf{x}, x_4 = a(N_\tau - 1)) \quad (8)$$

for all  $\mathbf{x}$  with an  $N_c \times N_c$  matrix,  $z_k = \text{diag}(e^{2\pi ik/N_c}, e^{2\pi ik/N_c}, \dots, e^{2\pi ik/N_c})$  where  $k = 0, 1, \dots, N_c - 1$ . (See figures 1 (a) and (b) for the graphical representation of the transformation.) Because this  $Z_{N_c}$  group is a centre of the  $SU(N_c)$  gauge group, the global symmetry under the transformation (8) is called centre symmetry and the Polyakov loop changes accordingly as  $L \rightarrow z_k L$ . Hence, the Polyakov loop expectation value is an order parameter for the spontaneous breaking of centre symmetry.

In general the expectation value of operator can be determined so as to minimise the effective potential. Therefore, the effective action  $\Gamma[\Phi]$  or the effective potential  $V[\Phi]$  would suffice to give the information on whether the system is in the confined or deconfined phase.

### 2.1. Perturbative approaches

Because the perturbative calculations are valid at such high temperature that gluons and quarks interact weakly, the deconfined phase should be favoured in the perturbative regime and  $\Phi \sim 1$  should be concluded. This anticipation was first confirmed by in [25, 26] in the  $SU(2)$  and  $SU(3)$  pure Yang-Mills theories. In the perturbative calculation it is more convenient to formulate the effective potential not in terms of  $\Phi$  directly but the phases of  $L$  instead.

In this article we shall limit ourselves to the simple case of colour  $SU(2)$  only. The generalisation to colour  $SU(3)$  is straightforward. Then, with an appropriate choice of the basis in colour space with which  $A_4$  is diagonal;

$$A_4 = \frac{2\pi T}{g} q \begin{pmatrix} 1 & 0 \\ 0 & -1 \end{pmatrix}. \quad (9)$$

The Polyakov loop matrix and its trace can be expressed in terms of  $q$  as

$$L = \begin{pmatrix} e^{i\pi q} & 0 \\ 0 & e^{-i\pi q} \end{pmatrix}, \quad \Phi = \langle \cos(\pi q) \rangle \quad (10)$$

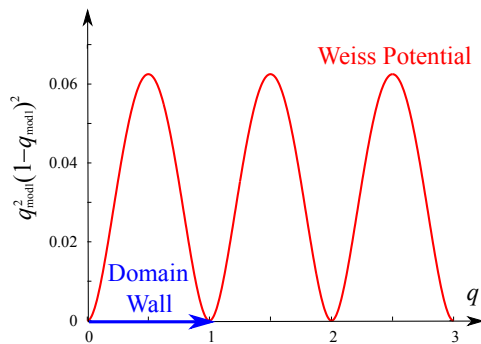


**Figure 2.** SU(2) Weiss potential as a function of  $q$  (rescaled  $A_4$ , i.e. the phase of the Polyakov loop). The domain wall configuration interpolates between two minima.

in the SU(2) case. Then, performing the one-loop integration on top of the  $A_4$  background, one can find the following expression;

$$V_{\text{eff}}^{(1)}[q] = VT \int \frac{d^3p}{(2\pi)^3} \left\{ \beta p + 2 \ln[1 - e^{-\beta p + 2i\pi q}] + 2 \ln[1 - e^{-\beta p - 2i\pi q}] \right\}, \quad (11)$$

where the Polyakov loop enters as an imaginary colour chemical potential. After dropping the zero-point energy and carrying the momentum integration out, one can arrive finally at the perturbative effective potential (namely the Weiss potential),

$$V_{\text{eff}}^{(1)}[q] = \frac{4\pi^2 V}{3\beta^4} q_{\text{mod}1}^2 (1 - q_{\text{mod}1})^2. \quad (12)$$

It is obvious from equation (11) that  $V_{\text{eff}}^{(1)}[q]$  is a periodic function of  $q$  with the period 1, that is the reason why  $q_{\text{mod}1}$  appears in equation (12). We remark that the Weiss potential is conveniently expressed by means of the Bernoulli polynomials. Figure 2 is a sketch of this periodic potential with the horizontal axis of  $q$ . In view of this periodic structure, one may well think of a tunnelling process that interpolates two minima. We will come to this point soon later.

The two-loop calculations were first attempted in references [27, 28], which turned out incomplete because the one-loop correction to the Polyakov loop had been missing; in the computation of the Polyakov loop, the tree-level relation,  $\langle \cos(\pi q) \rangle \approx \cos(\pi \langle q \rangle)$ , is insufficient for the two-loop potential. In this way, a simple prescription to treat the  $A_4$ -background as if it were the Polyakov loop itself has a potential risk of pitfall in the non-perturbative regime. This correction was taken into the SU(2) calculation first [29] and the SU( $N_c$ ) calculation later [30]. Although the complete expression for the SU( $N_c$ ) case has a complicated combination of the Bernoulli polynomials, it is reduced to a simple form in the SU(2) case. The effective potential of the two-loop order is composed from two pieces;  $V_f^{(2)}[q]$  from the direct contribution of the two-loop integration and  $V_p^{(2)}[q]$  from the Polyakov-loop renormalisation at one-loop order;

$$V_{\text{eff}}^{(2)}[q] = V_f^{(2)}[q] + V_p^{(2)}[q]. \quad (13)$$

They are individually calculated and the SU(2) results read;

$$V_f^{(2)}[q] = \frac{2\pi\alpha_s V}{\beta^4} \left[ q_{\text{mod}1}^2 (1 - q_{\text{mod}1})^2 - \frac{2}{3} q_{\text{mod}1} (1 - q_{\text{mod}1}) \right], \quad (14)$$

$$V_p^{(2)}[q] = -\frac{16\pi\alpha_s V}{3\beta^4} \left[ q_{\text{mod}1}^2 (1 - q_{\text{mod}1})^2 - \frac{1}{4} q_{\text{mod}1} (1 - q_{\text{mod}1}) \right]. \quad (15)$$

Adding these two potentials up, we find that the latter terms inside of the parentheses cancel out and the final expression simplifies as

$$V_{\text{eff}}^{(2)}[q] = -\frac{10\pi\alpha_s V}{3\beta^4} q_{\text{mod}1}^2 (1 - q_{\text{mod}1})^2. \quad (16)$$

Therefore, interestingly enough, the correction of the two-loop order modifies only the overall coefficient of the Weiss potential and does not alter the functional form of the potential. We can confirm that the perturbative vacuum at  $q = 0$  is indeed a minimum of the potential and then  $\Phi = +1$  is concluded from equation (10), which is not ruined by the correction (16).

From the Weiss potential, in the case when quarks are absent, the stable vacuum is degenerate at  $q = n$  with  $n$  being an integer, reflecting centre symmetry. These minima are, in fact, to be connected by the centre transformation. For general  $q = n$  the Polyakov loop takes a value of  $(-1)^n$ . This degeneracy between  $\Phi = +1$  and  $\Phi = -1$  would be broken by the presence of quarks.

The quark contribution to the Polyakov loop potential is known up to the two-loop order [30]. We explain only the one-loop result here. The one-loop integration reads, apart from the zero-point energy,

$$V_{\text{quark}}^{(1)}[q] = -4N_f VT \int \frac{d^3p}{(2\pi)^3} \left\{ \ln[1 + e^{-\beta p + i\pi q}] + \ln[1 + e^{-\beta p - i\pi q}] \right\}, \quad (17)$$

for massless  $N_f$  flavours, which eventually amounts to

$$V_{\text{quark}}^{(1)}[q] = -\frac{8N_f\pi^2 V}{3\beta^4} \left( \frac{q}{2} + \frac{1}{2} \right)_{\text{mod}1}^2 \left[ 1 - \left( \frac{q}{2} + \frac{1}{2} \right)_{\text{mod}1} \right]^2. \quad (18)$$

It is worth mentioning that one can recover the above functional form immediately by replacing  $q \rightarrow q/2 + 1/2$  in the Weiss potential (12). In this replacement an additional term  $1/2$  comes from the quantum statistics (boson or fermion) with which the exponential term changes the sign. Also, the argument is  $q/2$  instead of  $q$  because quarks belong to the colour fundamental representation, while gluons are in the adjoint representation. We will take a closer look at quark effects when we discuss the model studies at finite density in section 3.3.

Since the period is doubled as compared to the pure gluonic case, the potential has no degeneracy between  $\Phi = \pm 1$ . Thus,  $\Phi = 1$  (or  $q = 0$ ) is more favoured than  $\Phi = -1$ , which is a consequence of the explicit breaking of centre symmetry caused by quarks. In the presence of dynamical quarks, therefore, the state at  $\Phi = -1$  is a metastable vacuum. It is shown [31], however, that the metastable state has physically unacceptable properties in thermodynamics. Different Polyakov-loop domains, whose interface is the  $Z_{N_c}$  domain wall [32, 33], are meaningful only in Euclidean space. In

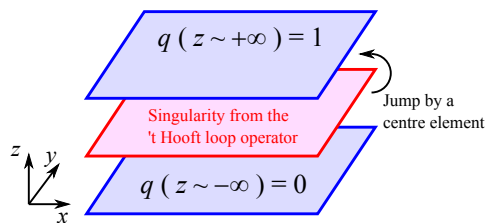


**Figure 3.** Schematic figure of the 't Hooft loop. A singularity on the surface  $\Sigma$  twists the boundary condition for the Polyakov loop by a centre element.

this interpretation the 't Hooft loop as we will discuss below is of special importance [34].

So far, we have considered only homogeneous configuration of the Polyakov loop background. One interesting application of the Weiss potential is the formation of the domain wall that is an inhomogeneous object in space. It is then convenient to introduce what is called the 't Hooft loop [35] (which measures the chromo-electric flux) besides the Wilson loop (which measures the chromo-magnetic flux). We denote the 't Hooft loop along the contour  $C$  as  $V(C)$  and then it should satisfy the operator relation;

$$V^\dagger(C)W(C')V(C) = e^{2i\pi Lk(C,C')/N_c}W(C') \quad (19)$$

with a centre-element coefficient in the right-hand side and Gauss' link number  $Lk(C, C')$  of the two contours  $C$  and  $C'$ . Mathematically  $Lk(C, C')$  can be expressed as [36]

$$Lk(C, C') = \frac{1}{4\pi} \oint_C dx_i \oint_{C'} dy_j \epsilon_{ijk} \frac{x_k - y_k}{|\mathbf{x} - \mathbf{y}|^3}, \quad (20)$$

which shall be easily understood from Ampère's law with the magnetic field given by Biot-Savart's law in electromagnetism. From the fact that the 't Hooft loop counts the chromo-electric flux, with a certain choice of the colour direction (which can be taken as the 3-rd direction in the SU(2) case without loss of generality), the explicit form of the 't Hooft loop could be given as [34]

$$V(C) = \exp \left[ \frac{2\pi i}{g} \int_\Sigma d^2 S^i E_i^3 \right], \quad (21)$$

where  $\Sigma$  is the two-dimensional sheet enclosed by  $C$ , i.e.  $\partial\Sigma = C$ . In the computation of the 't Hooft loop expectation value, the insertion of this operator to the functional integration induces a delta-function singularity (Dirac surface) on  $\Sigma$ , which makes a twist on the boundary condition for the Polyakov loop by a centre element  $z_k$  (that is  $-1$  for the SU(2) group). We illustrate a schematic picture in section 3.

With the choice of  $C$  in the whole  $x$ - $y$  plain, the surface  $\Sigma$  spans over the  $x$ - $y$  plane at a certain  $(z_0, t_0)$ . The expectation value of the 't Hooft loop is then given by [37]

$$\langle V(C) \rangle = \frac{Z_{\text{tbc}}}{Z_{\text{pbc}}}, \quad (22)$$

where  $Z_{\text{pbc}}$  is the partition function with the periodic boundary condition in the  $z$ -direction, while  $Z_{\text{tbc}}$  has a twisted boundary condition for the Polyakov loop.



Hence, to compute the expectation value of the 't Hooft loop, an effective action in terms of  $q$  is necessary including the derivative terms, that is given by

$$\Gamma_{\text{eff}}[q] = L_x L_y \int_0^{L_z} dz \left\{ \frac{2\pi^2}{g^2 \beta} \left[ \frac{dq(z)}{dz} \right]^2 + \frac{4\pi^2}{3\beta^3} q(z)^2 [1 - q(z)]^2 \right\}, \quad (23)$$

at one-loop order. This potential term is the Weiss potential and the derivative term is from the tree-level action. We note that the quantum corrections to the derivative term have been evaluated beyond the derivative expansion and a possibility of spatially inhomogeneous configuration of the Polyakov loop has been suggested [38].

In the presence of the 't Hooft loop, the twisted boundary condition is that  $q \rightarrow 0$  at  $z \rightarrow -\infty$  and  $q \rightarrow 1$  at  $z \rightarrow +\infty$ . The 't Hooft loop is a creation operator of centre-domain interface, therefore. The classical solution associated with the above effective action is

$$q_c(z) = \frac{1}{1 + \exp[-\sqrt{2/3}gTz]}, \quad (24)$$

which satisfies the boundary condition;  $q(z \rightarrow -\infty) = 0$  and  $q(z \rightarrow +\infty) = 1$ . Then, the effective action takes a finite value that is [32],

$$\Gamma_{\text{eff}}[q_c(z)] = \frac{4\pi^2}{3\sqrt{6}g\beta^2} L_x L_y = \sigma_t L_x L_y, \quad (25)$$

From this, the expectation value of the 't Hooft loop at the one-loop order is,

$$\langle V(C) \rangle = \exp[-\sigma_t \Sigma(C)] \quad (26)$$

with  $\Sigma(C) = L_x L_y$ , which shows the area law in the deconfinement phase. We see that the 't Hooft loop has behaviour opposite to the Wilson loop, and the 't Hooft loop plays the role of disorder parameter. Together with  $W(C)$  and  $V(C')$  the state of matter is characterised in more details as

$$\underline{\text{Confined Phase}} \quad \langle W(C) \rangle \sim e^{-\sigma_w \Sigma(C)}, \quad \langle V(C') \rangle \sim e^{-\sigma'_t L(C')}. \quad (27)$$

In the deconfinement phase, on the other hand, the behaviour is opposite;

$$\underline{\text{Higgs Phase}} \quad \langle W(C) \rangle \sim e^{-\sigma'_w L(C)}, \quad \langle V(C') \rangle \sim e^{-\sigma_t \Sigma(C')}. \quad (28)$$

In the Higgs phase at high temperature, there is no massless particle. It should be noted that all gluons are massive due to the thermal mass. Here, we can also consider the third possibility;

$$\underline{\text{Partial Higgs Phase}} \quad \langle W(C) \rangle \sim e^{-\sigma_w \Sigma(C)}, \quad \langle V(C) \rangle \sim e^{-\sigma_t \Sigma(C)}, \quad (29)$$

which represents the partial Higgs phase and confinement still remains. The last possibility that both the Wilson and the 't Hooft loops show the perimeter law is excluded from the operator algebra [35].

We have, so far, discussed the behaviour of the Wilson loop or the Polyakov loop as the order parameter and the spatial 't Hooft loop as the disorder parameter. The spatial Wilson loop is also an interesting quantity. For completeness we shall give a brief description about the spatial Wilson loop. It always shows the area law regardless of

the temperature. This can be understood in the 3-dimensional effective theory of QCD at high temperature [39] as a result of the dimensional reduction [40].

Integrating all “hard” modes out with non-zero Matsubara frequency at high temperature leaves a 3-dimensional effective theory of the “soft” length scales  $> (gT)^{-1}$ . This effective theory is commonly referred to as Electrostatic QCD (EQCD), that is defined by the Lagrangian,

$$S_{\text{EQCD}} = \int d^3x \left\{ \frac{1}{2} \text{tr} F_{ij} F_{ij} + \text{tr}(D_i A_0)^2 + m_{\text{E}}^2 \text{tr} A_0^2 + \lambda_{\text{E}} [\text{tr}(A_0^2)] + \bar{\lambda}_{\text{E}} \text{tr} A_0^4 \right\}. \quad (30)$$

The electrostatic field  $A_0(\mathbf{x})$  is static and adjoint scalar in colour space. The matching parameters in EQCD are calculated [41] and the three-loop level is still in progress [42, 43]. The leading-order results are to  $O(g^4)$ ;

$$g_{\text{E}}^2 = g^2(T)T, \quad m_{\text{E}}^2 = \frac{N_{\text{c}}}{3} g^2(T)T^2, \quad \lambda_{\text{E}} = \frac{N_{\text{c}} g^2(T)}{4\pi^2 N_{\text{c}}}, \quad \bar{\lambda}_{\text{E}} = \frac{N_{\text{c}} g^2(T)}{12\pi^2}. \quad (31)$$

Because  $A_0(\mathbf{x})$  is a heavily massive mode at high temperature, integrating  $A_0$  out leads to an effective theory of the “ultrasoft” length scales  $> (g^2 T)^{-1}$ , which is called Magnetostatic QCD (MQCD). This MQCD is defined by the Lagrangian,

$$S_{\text{MQCD}} = \int d^3x \frac{1}{2} \text{tr} F_{ij} F_{ij}. \quad (32)$$

This is a confining theory with the magnetic coupling constant, which is

$$g_{\text{M}}^2 = g_{\text{E}}^2 = g^2(T)T, \quad (33)$$

at the leading order. From the dimensional reason the string tension associated with this 3-dimensional effective theory is to be parametrised as

$$\sigma_{\text{s}} = c^2 g_{\text{M}}^4. \quad (34)$$

The determination of  $c$  requires full non-perturbative evaluation, and the Monte-Carlo simulation of the pure gluonic theory results in  $c \approx 0.553(1)$  [44, 45], which is also confirmed by later simulation [46].

Although systematic resummation programs in EQCD and MQCD are on the track, the Polyakov loop effects and confinement physics are not incorporated in a satisfactory manner (see reference [47] for some attempts). It is quite difficult to investigate the nature of deconfinement phase transition in the perturbative approaches.

## *2.2. Non-perturbative methods at work*

Theoretical researches on the confining properties near and below  $T_c$  require non-perturbative extensions of the method. The lattice-QCD simulations are the most successful as long as the quark chemical potential is sufficiently smaller than the temperature. For recent developments in the lattice-QCD calculations there are a number of nice reviews (see reference [48] for example). In this review article we shall focus on some of analytical approaches.

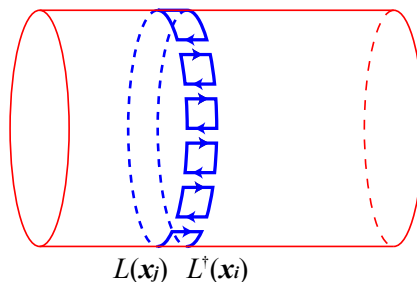


**Figure 4.** Leading order contribution to the Polyakov loop effective action in the strong-coupling limit.

*2.2.1. Strong-coupling expansion:* The deconfinement phase transition can be formulated non-perturbatively in the limit of the strong coupling constant,  $g^{-1} \rightarrow 0$ , which was first elucidated in the Hamiltonian formalism in reference [22]. The same conclusion is readily obtained in the formalism of functional integration [49, 50].

In the leading order of the plaquette expansion as sketched in figure 4, the effective action in terms of the Polyakov loop reads,

$$S_{\text{pol}}[L] = -e^{-\sigma a/T} \sum_{\text{n.n}} \text{tr} L^\dagger(\mathbf{x}_i) \text{tr} L(\mathbf{x}_j), \quad (35)$$

which describes a hopping interaction between adjacent Polyakov loops. Here  $a$  is the lattice spacing. This action actually defines a spin-like theory of the Polyakov loop matrix;

$$Z = \int \mathcal{D}L e^{-S_{\text{pol}}[L]}. \quad (36)$$

Here  $\mathcal{D}L$  represents the functional integral with the group invariant (Haar) measure. The theoretical content of this matrix model itself is very intriguing [51]. In the same manner as the mean-field treatment (or the so-called molecular-field approximation) of spin systems, it is possible to formulate the spontaneous breaking of centre symmetry and  $\Phi$  takes a finite value when the spin interaction becomes large at sufficiently high  $T$  [52, 53, 54, 55].

Although it is much simpler than the molecular-field approximation, the tree-level potential is already useful to describe the deconfinement phase transition. In this prescription the traced Polyakov loop in the action (35) is simply replaced by the expectation value  $\Phi$ , and an additional contribution comes from the Haar measure in the functional integration, i.e.

$$V_{\text{eff}}[\Phi] = -6V N_c^2 e^{-\sigma a/T} \bar{\Phi} \Phi - \ln \mathcal{M}_{\text{Haar}}[\Phi], \quad (37)$$

where the Haar measure for the  $\text{SU}(N_c)$  group is given by

$$\ln \mathcal{M}_{\text{Haar}} = \begin{cases} V \ln[1 - \bar{\Phi} \Phi], & (\text{for } N_c = 2) \\ V \ln[1 - 6\bar{\Phi} \Phi + 4(\bar{\Phi}^3 + \Phi^3) - 3(\bar{\Phi} \Phi)^2]. & (\text{for } N_c = 3) \end{cases} \quad (38)$$

It is important to note that these Haar measures favour the confining state at  $\Phi = 0$ . Moreover, the perturbative vacuum at  $\Phi = \pm 1$  has an infinitely high barrier, which is

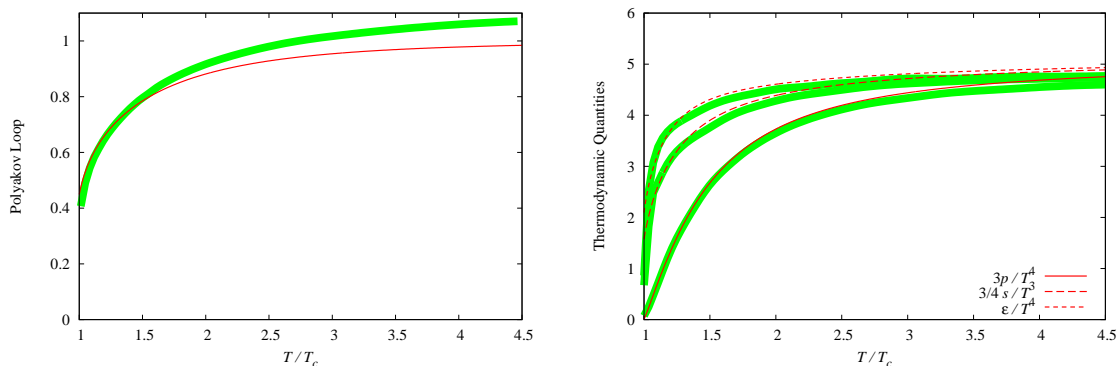


**Figure 5.** Left: Bands represent the lattice data for the Polyakov loop and the solid curve is the fitted result from equation (40). Right: Pressure, the entropy density and the internal energy density from lattice data and the fitted result. The lattice data is taken from reference [60] and the figure from reference [61].

cancelled by the longitudinal gluon loop in the perturbative calculation. Thus, the Haar measure could play an essential role in the realisation of confinement [56, 57]. Together with this Haar measure contribution and the spin interaction term, a phase transition takes place on the mean-field level and it is of second order for  $N_c = 2$  and of first order for  $N_c = 3$ . Here, we distinguish the anti-Polyakov loop,  $\bar{\Phi} = \langle \text{tr } L^\dagger \rangle / N_c$ , from  $\Phi$ ; they are just identical at zero baryon density but a discrepancy between them arises from finite-density effects and has much to do with the sign problem. We shall return to this problem in the next section.

The history of the investigations on chiral symmetry restoration in the strong-coupling expansion is as long as that of deconfinement physics, which is summarised in a review [58]. This section is devoted mainly to deconfinement physics and we will later look over the physics implications of chiral dynamics in section 3.

Inspired by the functional form from the strong-coupling analysis, one can adopt the following Ansatz to fit the pressure in the pure gluonic sector;

$$V(\Phi) = -\frac{a(T)}{2}\bar{\Phi}\Phi + b(T)\ln\left[1 - 6\bar{\Phi}\Phi + 4(\bar{\Phi}^3 + \Phi^3) - 3(\bar{\Phi}\Phi)^2\right], \quad (39)$$

where a set of parameters,  $a(T)/T^4 = 3.51 - 2.47t^{-1} + 15.2t^{-2}$  and  $b(T)/T^4 = -1.75t^{-3}$  with  $t = T/T_c$ , can reproduce the lattice data well [59]. In this parametrisation there are only three free variables because one of four is constrained by the Stefan-Boltzmann law. It is amazing that not only the Polyakov loop but also the pressure estimated from

$$\left.\frac{dV(\Phi)}{d\Phi}\right|_{\Phi=\Phi_0} = 0, \quad P = V(\Phi = \Phi_0), \quad (40)$$

simultaneously agree well with the lattice data [60], as seen in the plots in figure 5.

The agreement is impressive for only three fitting parameters, except for the Polyakov loop at very high temperature. The Polyakov loop from the lattice data exceeds unity there, which is caused by the renormalisation effect on the Polyakov loop

[62, 63, 64, 60]. It is known that the UV divergence in the Polyakov loop is absorbed by the charge renormalisation as

$$\Phi^{\text{ren}}(T) = [Z(g^2)]^{N_\tau} \Phi^{\text{bare}}(g^2, N_\tau). \quad (41)$$

The renormalisation constant is fixed at a reference temperature, that corresponds to the renormalisation condition. Once this is done in a certain scheme, a renormalisation constant at a different temperature is fixed by a different  $N_\tau$ , which in turn leads to the renormalisation constant at a different coupling  $g$  (or lattice spacing). In this way the normalised Polyakov loop is calculated for all temperatures through the iterative procedure. It is a non-trivial question how to incorporate the renormalisation effect in the Polyakov loop model [65].

*2.2.2. Large- $N_c$  QCD:* The confinement-deconfinement transition is well-defined only in the pure Yang-Mills theories without quarks in the colour fundamental representation or in the limit of infinite quark mass. Otherwise, in the presence of dynamical quarks, centre symmetry is explicitly broken and the Polyakov loop always takes a finite value;  $\Phi \neq 0$ . The Polyakov loop correlation function, in other words, does not decay exponentially at large distances due to pair creation of quark and anti-quark.

Even in the presence of dynamical quarks, however, there is another limit in which the deconfinement transition is well-defined. That is, increasing the number of gluons instead of decreasing the number of quarks. In fact the quark contribution is relatively suppressed than gluons with large number of colours  $N_c \rightarrow \infty$  [66, 67], and eventually, in the limit of infinite colours a smooth crossover of deconfinement turns into a sharp phase transition.

If we see the pressure of finite- $T$  hadronic matter, on the one hand, it is of  $O(1)$  in the  $N_c$  counting. There are gluons of  $O(N_c^2)$ , on the other hand, and the pressure of deconfined matter is of  $O(N_c^2)$ . This is dominant over the quark contribution of  $O(N_c)$ . Therefore, in the limit of  $N_c \rightarrow \infty$ , the quark contribution becomes negligible and the quenched approximation works correctly. The pressure then jumps from  $O(1)$  to  $O(N_c^2)$  when the system goes through the phase transition from the hadronic to the deconfined phases. This means that the location of the phase transition has no ambiguity unlike the pseudo-critical temperature of crossover at  $N_c = 3$ .

It is a subtle question what the order of the phase transition would be in the  $N_c \rightarrow \infty$  limit. One might have thought that the phase transition should be of first order simply because of a big jump in the pressure. It is, however, possible to have a second (or higher) order phase transition with a pressure that is continuous but increasing rapidly. There are, hence, two naive possibilities: (1) The phase transition (or crossover) is continuous for any  $N_c$  and the  $N_c \rightarrow \infty$  limit makes it of second order. (2) The phase transition at  $N_c \rightarrow \infty$  is of first order and there is a critical number of colours at which the phase transition is of exact second order.

The fact seems to be more complicated. In the large- $N_c$  limit of the Polyakov loop matrix model another possibility has been suggested; the Gross-Witten point could be

realised at  $N_c \rightarrow \infty$  [68]. Then the effective potential is flat in the region  $0 \leq \Phi < 1/2$  and starts increasing for  $\Phi \geq 1/2$ . The Polyakov loop jumps from 0 to 1/2 at the critical point. This is an unconventional point because no interface tension is needed for a jump between  $\Phi = 0$  and  $\Phi = 1/2$ , which would turn into a continuous transition immediately with an infinitesimal background.

The large- $N_c$  approach is useful as long as dropping dynamical quarks off is not critically harmful. It is an interesting theoretical challenge to apply the large- $N_c$  argument for finite-density problems.

*2.2.3. Holographic model:* The application of the AdS/CFT correspondence has become an important building block of hot and dense QCD physics. The idea is that the weak-coupling Type-IIB supergravity theory on  $\text{AdS}_5 \times S^5$  is equivalent to the strong-coupling  $\mathcal{N} = 2$  super Yang-Mills theory on the boundary of  $\text{AdS}_5$  space. Especially the presence of the QGP is translated into a non-extremal black-hole solution (see references [69, 70] for reviews). This technique is quite useful to examine non-perturbative aspects of strong-coupling gauge theories. The problem in the application to QCD physics is that QCD is neither conformal invariant nor supersymmetric. There are a number of theoretical attempts to design the black-hole solution so that it can mimic QCD thermodynamics [71, 72] with a hope to establish the AdS/QCD model.

One of the simplest ways to introduce a mass scale is to use the following Ansatz for the five-dimensional background geometry (in Einstein frame);

$$ds^2 = e^{cz^2} \frac{L^2}{z^2} \left[ -f(z) dt^2 + d\vec{x}^2 + f^{-1}(z) dz^2 \right] \quad (42)$$

with  $f(z) = 1 - (z/z_h)^4$ , which describes a Schwarzschild-type black hole along the fifth coordinate  $z$ . The corresponding Hawking temperature is

$$T = \frac{1}{\pi z_h} , \quad (43)$$

that is interpreted as the QGP temperature in the gauge theory side. The dilaton potential contains a dimensional parameter  $c$  that plays the role of QCD scale in this model. Such a model is usually referred to as the soft-wall model (usually defined in string frame) and is quite successful to give a semi-quantitative description of the Regge trajectory in the vector-meson channel [73] (see also reference [74] for a related approach). This type of approach is generally called the bottom-up model.

Interestingly enough, the deconfinement phase transition is clearly identified in such a holographic setup. The QGP at high temperature is featured by the metric (42), whereas confined matter at zero temperature is described by the metric with  $z_h \rightarrow \infty$  (and thus  $T \rightarrow 0$ ). Then, the five-dimensional actions associated with respective metrics determines which state is energetically favoured. In the soft-wall model the critical temperature  $T_c$  has been obtained as  $T_c \simeq \sqrt{c}/\pi$  [75, 76] when the Hawking-Page transition takes place. It is noteworthy that this phase transition of deconfinement is almost always of first order (see [71] for a possibility of exception).

The Polyakov loop expectation value is calculated by the string world-sheet area that is minimised with the boundary along the Polyakov loop [77]. It follows that

$$\Phi(T) = \exp \left[ a - b \left\{ \sqrt{\pi} \frac{T_c}{T} \operatorname{Erfi} \left( \frac{T_c}{T} \right) + 1 - e^{(T_c/T)^2} \right\} \right], \quad (44)$$

where  $a$  is a normalisation constant and  $b = R^2/2\alpha'$  is a parameter in the Nambu-Goto string action. A choice of  $a = 0.10$  and  $b = 0.72$  fits the lattice data very well.

As long as the Polyakov loop behaviour and bulk thermodynamic quantities are concerned, the results from the holographic approach are no better than the strong-coupling expansion as we have seen in equation (40). It should be an advantage in the holographic model that some quantities that cannot be calculated on the lattice can be calculated easily such as the transport coefficients [78, 79]. Indeed, the computation of the shear viscosity in the strong-coupling expansion has not been successful particularly including the effect of the deconfinement transition [80].

### 3. Baryon-Rich State of QCD

Historically speaking, the possibility of deconfined gluons and quarks was pointed out first for physics not at high temperature but at high density in the context of neutron star structure [81, 82]. It is, however, a non-trivial question whether the QCD running coupling constant really gets smaller at higher baryon density, as compared to the finite- $T$  case in section 2. Because quark excitations are allowed only outside of the Fermi sphere if  $T$  is small, dynamical quarks must carry as large momentum as the quark chemical potential  $\mu_q$ . The important point is that the relevant scale in  $\alpha_s(\mu)$  in equation (2) is not the momentum of quarks but that of the exchanged gluon between quarks. It is still possible for fast-moving quarks to emit and absorb soft gluons, for which  $\mu$  could be small and  $\alpha_s(\mu)$  could be substantially large. Such soft processes are, however, screened immediately due to quark polarisation effects that induce a screening mass  $\sim g\mu_q$  on gluons. In this way, in effect, one can regard sufficiently high-density matter of QCD as a weak-coupling system. This way of understanding is challenged recently by the large- $N_c$  approach to the QCD phase diagram as we will see later in section 3.2.2.

It is an ongoing project of experiment to explore the state of QCD matter in a wide range of temperature and baryon density by varying the collision energy  $\sqrt{s_{NN}}$ . From the phenomenological analysis using the thermal Statistical Model [83, 84, 85] a set of the temperature  $T$  and the baryon chemical potential  $\mu_B (= 3\mu_q)$  at which the chemical composition of particle species is frozen has been extracted. These “chemical freeze-out points” are very well parametrised by [83]

$$T_f(\mu_B) = a - b\mu_B^2 - c\mu_B^4 \quad (45)$$

with  $a = 0.166 \pm 0.002$  GeV,  $b = 0.139 \pm 0.016$  GeV<sup>-1</sup> and  $c = 0.053 \pm 0.021$  GeV<sup>-3</sup>. Also the baryon chemical potential at chemical freeze-out is parametrised as a function

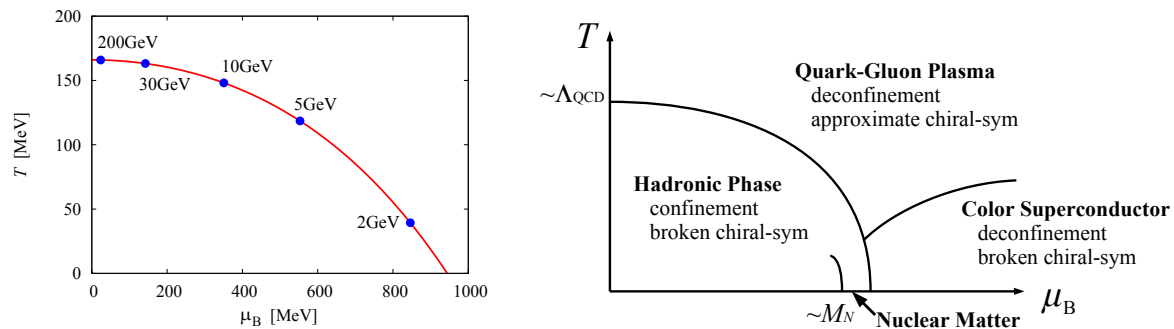


**Figure 6.** Left: Chemical freeze-out line. In the figure arbitrary five points are picked up to show the collision energy dependence of the chemical freeze-out point. Right: Minimal structure of the QCD phases in the  $\mu_B$ - $T$  plane. The critical  $T$  is of order  $\Lambda_{\text{QCD}}$  and the critical  $\mu_B$  is near the nucleon mass which is of order  $N_c \Lambda_{\text{QCD}}$ .

of the collision energy as

$$\mu_f(\sqrt{s_{NN}}) = \frac{d}{1 + e\sqrt{s_{NN}}} \quad (46)$$

with  $d = 1.308 \pm 0.028$  GeV and  $e = 0.273 \pm 0.008$  GeV $^{-1}$ , from which one can convert equation (45) into  $T_f(\sqrt{s_{NN}})$  easily.

These parametrisations are useful to relate theoretical predictions (for example, fluctuations of the charged particles, the baryon number etc; see reference [86]) to experimental observable as a function of not only  $\mu_B$  but also  $\sqrt{s_{NN}}$  that is under experimental control.

It is a natural anticipation that this chemical freeze-out line, which is plotted in the left of figure 6, is related to the colour deconfinement phenomenon that causes a rapid increase in the particle number density, and thus the multiparticle scattering rate [87]. We note that chiral symmetry restoration is not taken into consideration at all in the assumption of the thermal Statistical Model. In this way a part of the theoretically conjectured QCD phase diagram (the right of figure 6) has been backed up by experimental data, which should be complemented further by a line associated with colour superconductivity (see reference [88] for a modern review and references therein). We should emphasise that figure 6 shows only the minimal structure of possible QCD phases. There are many other possibilities on top of this minimal topology, some of which are summarised in my previous review [11].

Progresses in the experimental activities towards QCD matter at higher baryon density are strongly needed by theorists. Unlike the case at high  $T$  and small  $\mu_B$ , theoretical works have not been successful to make any robust prediction on the baryon-rich state of QCD matter. It is absolutely necessary to constrain proposed theoretical possibilities from the experimental point of view.



### 3.1. Perturbative approaches and problems

Let us first consider an extension of the Weiss potential (12) to the finite-density case. We can perform the perturbative integration as in the standard procedure with a quark chemical potential  $\mu_q$  introduced [89, 90, 91]. It seems at a first glance that such extension is straightforward, but it is not so simple once the Polyakov loop background is involved.

The loop corrections to the Weiss potential have been evaluated with dynamical (massless) quarks. The one-loop contribution from massless quarks is modified by  $\mu_q$  from equation (17) into

$$V_{\text{quark}}^{(1)}[q] = -2N_f VT \int \frac{d^3p}{(2\pi)^3} \sum_j \left\{ \ln[1 + e^{-\beta p + \beta \mu_q + i\pi q_j}] + \ln[1 + e^{-\beta p - \beta \mu_q - i\pi q_j}] \right\}, \quad (47)$$

which is generalised from SU(2) to SU( $N_c$ ) with  $j$  running from 1 to  $N_c$  (and  $\sum_j q_j = 0$ ). The first and second logarithms represent the particle and the anti-particle excitations, respectively. Then, the result after the momentum integration is obtained immediately [92] by the replacement of

$$q_j \rightarrow q_j - i \frac{\mu_q}{\pi T} \quad (48)$$

in equation (18).

This final result is simple but astonishing. Unless the gauge group is SU(2), the effective potential generally takes a complex value. How can one determine the energetically favourite value of  $q_j$  from such a complex potential? One might have thought that  $q_j$  should minimise the real part of the potential. Although such a working hypothesis may give a practical prescription, this cannot be justified from the first-principle approach. This complex potential for the Polyakov loop is one clear manifestation of the notorious sign problem (see reference [93] for an introductory review).

The sign problem hinders the lattice-QCD simulation at finite density. Contrary to what is believed, the sign problem is actually a quite generic problem of the importance sampling not only in the lattice-QCD simulation but in the mean-field approximation also [94, 95]. One should notice that the mean-field approximation is based on the importance sampling; the mean-field variables are chosen to be a ‘‘configuration’’ that maximises the weight  $\sim e^{-V_{\text{eff}}[q]}$ . When the potential is complex, therefore, the mean-field approximation breaks down.

Occasionally, in some analytical studies, it is overemphasised that the method be sign-problem free. Such a statement must be misleading as long as the method relies on the mean-field approximation for the treatment of the gauge-field part such as the Polyakov loop dynamics.

### 3.2. Non-perturbative methods in progress

One of the most urgent challenges in theory is to limn the global structure of the QCD phase diagram and fill in the quantitative details on figure 6. Non-perturbative methods

are indispensable to access the information in the vicinity of phase transition regions. There are significant progresses recently in the strong-coupling expansion, the large- $N_c$  QCD and the effective models to shed light on the phase diagram. Unfortunately, not much about the phase diagram can be said from the holographic QCD models, though there are many interesting attempts on each state of QCD matter, particularly by means of the AdS-Reissner-Nordström black hole [96, 97, 98, 99], where the charged black hole in AdS space is identified as the finite- $T$  and finite- $\mu_q$  plasma.

*3.2.1. Strong-coupling expansion and the matrix model:* The Polyakov loop matrix model emerges as a result of the strong coupling expansion and this model provides us with an ideal setup to think of the sign problem. In the leading order of the hopping parameter expansion [100], in the presence of heavy quarks, the quark-loop contribution or the Dirac determinant amounts to

$$\mathcal{M}_{\text{quark}}(\mu_q) \approx 1 + h \sum_{\mathbf{x}} \left[ e^{\beta\mu_q} \text{tr} L(\mathbf{x}) + e^{-\beta\mu_q} \text{tr} L^\dagger(\mathbf{x}) \right] \quad (49)$$

with a coefficient  $h$  which is small for large quark mass  $m_q$  and eventually  $\mathcal{M}_{\text{quark}}(\mu_q) \rightarrow 1$  as  $m_q \rightarrow \infty$  (quenched limit). Because the Polyakov loop changes non-trivially under a centre transformation, the above quark contribution breaks centre symmetry explicitly. Besides, this action becomes complex when a finite  $\mu_q$  is turned on since  $\text{tr} L$  takes a complex value in general.

The expression (49) is very useful to grasp the nature of the sign problem. One can also use equation (49) the other way around to deduce special situations where the sign problem weakens. We shall enumerate some of widely acknowledged examples here:

- Two-colour QCD [101, 102, 103] — If the colour gauge group is  $SU(2)$ , the Polyakov loop is always real;  $\text{tr} L = \text{tr} L^\dagger = 2 \cos(\pi q)$ . Equation (49) is thus real. Taking a real value is not sufficient for feasibility of the importance sampling because the Dirac determinant could be real but negative. There must be an even number of degenerate quark species in order to guarantee the semi-positivity of the Dirac determinant.
- Isospin Chemical Potential [104, 105] — We see that  $\mathcal{M}_{\text{quark}}(-\mu_q) = \mathcal{M}_{\text{quark}}(\mu_q)^*$  from equation (49), meaning that the whole Dirac determinant is semi-positive definite if there are two degenerate quarks that have a chemical potential opposite to each other. For example,  $\mu_u = \mu_I$  for  $u$ -quarks and  $\mu_d = -\mu_I$  for  $d$ -quarks with  $m_u = m_d$ . It is then easy to confirm that the Dirac determinant satisfies,

$$\mathcal{M}_{\text{quark}}(\mu_u) \mathcal{M}_{\text{quark}}(\mu_d) = |\mathcal{M}_{\text{quark}}(\mu_I)|^2 \geq 0. \quad (50)$$

The isospin chemical potential causes no sign problem, therefore, and the Monte-Carlo simulations are feasible. The absence of the sign problem for the chiral chemical potential  $\mu_5$  is also a variant of this category [106], for which some lattice simulations are successful [107, 108].

- Imaginary Chemical Potential [109, 110, 111] — The sign problem originates from the imbalance between the quark and anti-quark propagation in equation (49), which can be made balanced by replacing  $\mu_q$  by a pure-imaginary quantity  $i\tilde{\mu}_q$ . Then  $\mathcal{M}_{\text{quark}}(\tilde{\mu}_q)$  is obviously real. In this case, unlike two-colour QCD, there needs not be an even number of degenerate quark species because  $e^{i\beta\tilde{\mu}_q}$  is bounded. (The situation about the positivity of the Dirac determinant is rather similar to the zero-density case.) One may have thought that the Dirac determinant is then a periodic function of  $\tilde{\mu}_q$  with a period  $2\pi T$ . This is not correct. In fact the phase factor  $e^{i\beta\tilde{\mu}_q}$  can be partially cancelled by the centre transformation and the rest takes a value from 1 to  $e^{2i\pi/N_c}$ . This means that the genuine period is  $2\pi T/N_c$  instead of  $2\pi$  (i.e. Roberge-Weiss periodicity [112]).

Even though the sign problem is not washed away, the mean-field approximation works anyway (see section 3.3 for details). In the strong-coupling expansion the gauge action is dropped and the quark sector is dominant. Then, it is not the deconfinement transition but the chiral phase transition that defines the phase diagram. The phase boundary of chiral restoration obtained by means of the staggered formalism of chiral fermions [58, 113, 114] is in qualitative agreement with figure 6, which has been also confirmed by the numerical simulation [115].

The effect of the Polyakov loop dynamics as formulated by the action (35) has been taken into account too [52, 53, 54, 55]. Such a treatment on the lattice can be easily translated into the continuum language, which has led to the so-called PNJL-type models as we discuss soon below.

*3.2.2. Large- $N_c$  QCD:* Recently an interesting possibility about a new structure on the QCD phase diagram has been suggested from analytic deliberations on the large- $N_c$  limit of QCD at finite  $T$  and  $\mu_B$  [116]. The phase diagram takes a simple structure as sketched in figure 7 with three regions separated by straight first-order phase boundaries.

In the large- $N_c$  limit quark loops are suppressed by  $1/N_c$  as compared to gluon loops, so  $\mu_B$  does not affect the deconfinement transition line which is predominantly determined by  $N_c^2 - 1$  gluons. Hence the deconfinement transition makes a straight line parallel to the  $\mu_B$  axis. A free quark gas would give a pressure of  $\sim N_c \mu_q^4 \sim N_c^{-3} \mu_B^4$ , and thus the deconfinement transition line would be deformed for  $\mu_B$  as large as  $O(N_c^{5/4})$  that surpasses the gluon degrees of freedom. Before this is reached, there appears another type of transition at  $\mu_B \simeq M_N$  where  $M_N$  is the lightest baryon excitation energy (baryon mass minus binding energy). The baryon number density becomes non-vanishing then and the system pressure jumps from  $O(N_c^0)$  in the hadronic phase to  $O(N_c)$  in the new phase which is called Quarkyonic Matter. Before the deconfinement phase transition takes place with  $T \sim \Lambda_{\text{QCD}}$ , glueballs and mesons cannot affect this threshold for the baryon number and so the threshold located at  $\mu_B \simeq M_N$  makes a straight line parallel to the  $T$  axis, which results in the phase structure presented in figure 7.

The reason why the right-bottom region of figure 7 is identified as the Quarkyonic

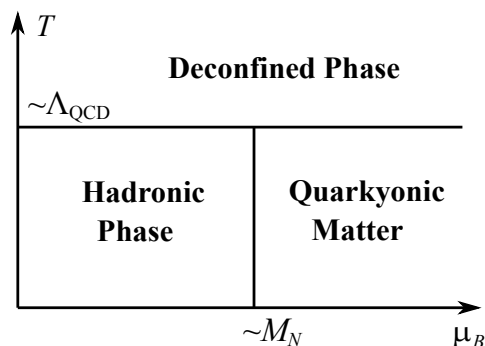


**Figure 7.** The phase diagram of large- $N_c$  QCD [116]. The hadronic phase confines coloured excitations and only glueballs and mesons exist. The corresponding system pressure is of  $O(N_c^0)$ . Above the deconfinement temperature of order of  $\Lambda_{\text{QCD}}$ , thermal excitations are dominated by gluons and the associated pressure is of  $O(N_c^2)$ . The quarkyonic phase is characterised by the pressure of  $O(N_c)$  at  $\mu_B$  greater than the lightest baryon mass  $M_N$  so that the baryon number density is non-vanishing.

Matter is the following. As explained before, gluons and quarks are all confined below the deconfinement transition line, and so the Quarkyonic Matter region resides in the confined regime. Therefore the physical degrees of freedom there should be baryons rather than quarks, and one can prove that the dense baryonic system at large  $N_c$  indeed gives the pressure of  $\sim O(N_c)$  whose major contribution comes from not the Fermi energy but the baryon-baryon interaction energy [116]. On the other hand, a gas of quarks naturally yields a pressure of  $O(N_c)$  because of the presence of  $N_c$  quarks. Such coincidence in the  $N_c$  counting implies that this bottom-right state would confine quarks and nevertheless feel quarks somehow. In other words a dual interpretation is possible; matter of strongly-interacting baryons and that of weakly-interacting quarks, which motivated the name, Quarkyonic Matter = (Quark + Baryonic) Matter.

Such an interpretation may sound peculiar but there is a reasonable way to reconcile two interpretations in terms of baryons and quarks. That is, particles sitting deeply inside the Fermi sea cannot be a part of excitation spectra, and so they could be quarks even though the system is in the confined phase. Therefore, the Fermi sphere consists of both baryons and quarks; baryons in the momentum layer  $\sim \Lambda_{\text{QCD}}$  near the Fermi surface (but, because of the confining interaction, there is no sharp Fermi surface in reality) and quarks inside of the Fermi sphere which does not take part in the excitation but gives the pressure of  $\sim O(N_c)$ .

This is actually what should be expected in the large- $N_c$  limit. As we have discussed in the beginning of this section, a large  $\mu_q$  does not guarantee the smallness of  $\alpha_s(\mu_q)$ , but the screening effects due to quark polarisation make  $\alpha_s(\mu)$  effectively small enough to realise the perturbative regime at high density. Because the quark loops are suppressed in the  $N_c$  counting, the screening effects would diminish and soft-gluon exchange would become important for large  $N_c$ .

The soft-gluon exchange would lead to confinement for excitations on top of the

Fermi surface, and furthermore, to an interesting consequence for the chiral-symmetry breaking mechanism [117, 118]. Usually the homogeneous chiral condensate  $\langle \bar{q}q \rangle$  or the condensation of the sigma meson is attributed to the spontaneous breaking of chiral symmetry. Because quarks and quark-holes must sit near the Fermi surface, if the net momentum of  $\bar{q}q$ -system is zero on the one hand, the gluon exchanged between a quark and a quark-hole on the Fermi surface must carry as large momentum as  $2\mu_q$ . On the other hand, this momentum can be absorbed in the net momentum of  $\bar{q}q$ -system and then the possible soft-gluon exchange favours an inhomogeneous chiral condensate, namely, the chiral spiral state.

It is a subtle question whether the chiral spiral structure emerges in the real world at  $N_c = 3$  and Quarkyonic Matter exists. This depends on the competition of the strength of confining force and the screening due to quark polarisation. For the sake of such quantitative clarification the effective model study was expected to hint the relevance or irrelevance of the large- $N_c$  limit to the real world. It has turned out, however, that one should inevitably go beyond the mean-field approximation and it is still a very difficult question how to resum the Polyakov loop fluctuations.

### *3.3. Extrapolation from effective models*

The Polyakov loop behaviour in the pure gluonic sector is described nicely by the simple parametrisation (39). The quark loop on top of the Polyakov loop background in equation (47) is expressed in a gauge invariant way, i.e.

$$V_{\text{quark}}^{(1)} = -2N_f VT \int \frac{d^3p}{(2\pi)^3} \left\{ \text{tr} \ln[1 + L e^{-\beta(\epsilon - \mu_q)}] + \text{tr} \ln[1 + L^\dagger e^{-\beta(\epsilon + \mu_q)}] \right\}, \quad (51)$$

where the quark mass is included in the energy dispersion relation  $\epsilon = \sqrt{p^2 + M_q^2}$  with the dynamically generated mass  $M_q$  which could be considerably larger than  $\mu_q$ . This form of the coupling is simple but has rich contents. If chiral symmetry is badly broken by large  $M_q$ , the exponential terms are small and thus the Polyakov loop coupling to the chiral sector diminishes, which is in favour of confinement. If the Polyakov-loop expectation value is small, on the other hand, the thermal excitation of quarks is severely screened and thus chiral restoration is delayed.

Interestingly enough, the colour trace in equation (51) is explicitly taken to be a form of

$$V_{\text{quark}}^{(1)} = -2N_f VT \int \frac{d^3p}{(2\pi)^3} \left\{ \ln \left[ 1 + \text{tr} L e^{-\beta(\epsilon - \mu_q)} + \text{tr} L^\dagger e^{-2\beta(\epsilon - \mu_q)} + e^{-3\beta(\epsilon - \mu_q)} \right] \right. \\ \left. + \ln \left[ 1 + \text{tr} L^\dagger e^{-\beta(\epsilon + \mu_q)} + \text{tr} L e^{-2\beta(\epsilon + \mu_q)} + e^{-3\beta(\epsilon + \mu_q)} \right] \right\}. \quad (52)$$

The further missing piece in the dynamics is the spontaneous breaking of chiral symmetry now that the deconfinement and coupling parts are formulated as explained above. The Polyakov-loop coupled Nambu–Jona-Lasinio model (PNJL model) [119, 120] utilises the NJL model as a dynamical theory to describe the chiral condensate  $\langle \bar{q}q \rangle$ . Replacing the NJL model by another successful chiral model, the Quark-Meson (QM)

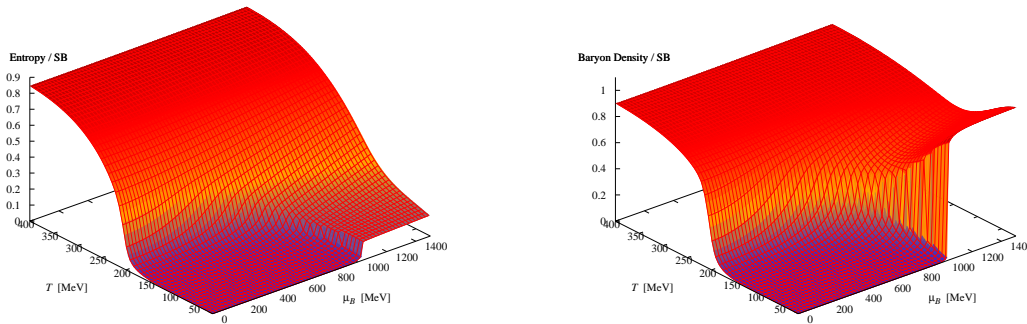


**Figure 8.** Entropy density and the quark number density normalised by the Stefan-Boltzmann limit in the mean-field approximation of the PNJL model.

model (that is a variant of the linear sigma model), one can define the PQM model [121]. In the simple mean-field approximation the PNJL model is more convenient than the PQM model because the linear sigma model suffers from artificial first-order phase transition [122]. This model artifact is cured by pion loop effects implemented by the renormalisation group (RG) improvement. For this purpose of RG studies the PQM setup has an advantage over the PNJL model [123, 124].

So far the RG improvement on the meson fluctuations has been well investigated, while it is not known how to include the Polyakov loop fluctuations systematically. Once the Polyakov loop potential is given, there is no way to improve it, and a more fundamental starting point is necessary. One possibility is to take the Polyakov loop matrix model that can in principle encompass soft fluctuations of the Polyakov loop. Since this matrix model is defined on the lattice, however, it is technically difficult to accomplish the RG analysis. Another possibility is to postulate a derivative term in the Polyakov loop action, i.e. setup of the so-called Polyakov loop model [125] and to put it in the RG equation [126].

Here, let us make a brief remark on the sign problem in the PNJL-type models. It may seem to be sign-problem free in equation (52) but it is not so. In the simple mean-field analysis equation (52) leads to

$$V_{\text{quark}}^{(1)}[\Phi, \bar{\Phi}] = -2N_f VT \int \frac{d^3p}{(2\pi)^3} \left\{ \ln \left[ 1 + 3\Phi e^{-\beta(\epsilon - \mu_q)} + 3\bar{\Phi} e^{-2\beta(\epsilon - \mu_q)} + e^{-3\beta(\epsilon - \mu_q)} \right] + \ln \left[ 1 + 3\bar{\Phi} e^{-\beta(\epsilon + \mu_q)} + 3\Phi e^{-2\beta(\epsilon + \mu_q)} + e^{-3\beta(\epsilon + \mu_q)} \right] \right\}. \quad (53)$$

Here, at finite  $\mu_q$ , it is necessary to treat  $\Phi$  and  $\bar{\Phi}$  independently. Then, one can plot  $V_{\text{quark}}^{(1)}[\Phi, \bar{\Phi}]$  as a function of  $\Phi$  and  $\bar{\Phi}$  to recognise a funny shape. In particular one may find that the solution of the gap equation is not stable in the direction of  $\bar{\Phi} - \Phi$ . This is how the sign problem remains unsolved in the mean-field model study [95].

Nevertheless, once an approximation is made with a prescription to adopt the solution of the gap equation, the model results are useful to figure the thermodynamic quantities out at finite  $T$  and  $\mu_B$ . Figure 8 shows some examples from the PNJL model

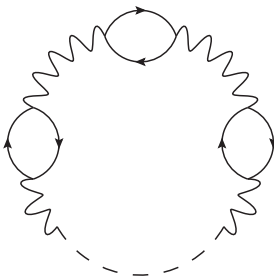


**Figure 9.** Ring diagram of gluons with the quark pair creation/annihilation. The Polyakov loop potential must have coupling to the quark chemical potential  $\mu_q$  through this quark polarisation. If an external  $\mathbf{B}$  is applied, gluons can feel  $\mathbf{B}$  through this diagram too.

in the simple mean-field approximation [127]. The left is the entropy density divided by the Stefan-Boltzmann limit and the right is the baryon number density divided by the Stefan-Boltzmann limit. Naturally the increase in the entropy density is to be interpreted as deconfinement. One may well conclude that the model results could have implied the realisation of Quarkyonic Matter at low  $T$  and high  $\mu_B$  where the entropy density stays small and the baryon density gets large which is characteristic to Quarkyonic Matter.

However, the model study has missing diagrams, as depicted in figure 9, which is not included even in the RG improvement and is related to the Polyakov loop fluctuations. This missing contribution is critically important to clarify the QCD phase structure including the possibility of Quarkyonic Matter. Without this diagram the Polyakov loop potential (39) has no explicit dependence on  $\mu_q$ , so that the deconfinement transition is almost insensitive to  $\mu_q$  even with the coupling effects through equation (51). This approximate  $\mu_q$ -independence is observed in the entropy behaviour too in the left of figure 8. Then, the phase diagram from the PNJL or PQM models turns out similar to the large- $N_c$  conjecture in figure 7. In fact, the polarisation effects in figure 9 are suppressed in the large- $N_c$  limit.

It is not straightforward to implement the polarisation effects properly in the effective model without losing simplicity. The model is to be appreciated as long as it is simple enough to deepen the intuition of physics understanding. There are only a few attempts to incorporate effects originating from the diagram in figure 9 into the PNJL-type models. By the hypothetical matching condition for the deconfinement and chiral transitions the  $\mu_q$ -dependence was introduced in reference [121]. Then, the deconfinement line comes along with the chiral restoration line on the phase diagram, but this statement is a consequence by construction of the model. In reference [128] the  $\mu_q$ -dependence in the Polyakov loop potential was determined by the matching condition to thermodynamics from the thermal Statistical Model, which has confirmed quantitative agreement with the prescription in reference [121].

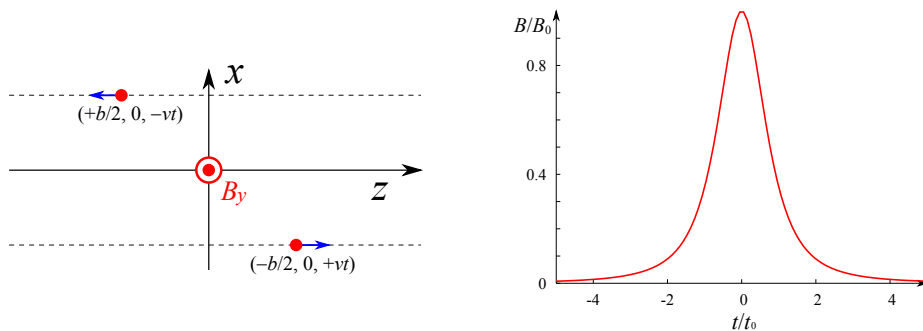


**Figure 10.** Left: Collision geometry seen from the above. Right: Profile of the produced magnetic field as a function of time.

This kind of polarisation effect is of increasing importance in the researches on finite-density QCD matter. Besides, as we see in the next section, QCD in strong magnetic fields is currently a hot subject and it requires detailed information on the polarisation effect. The reason for this is exactly the same as the finite-density case. Gluons do not feel the magnetic fields directly, but do see them through the quark polarisation as in figure 9.

#### 4. Strong Magnetic Field and Dimensional Reduction

In the heavy-ion collision with a finite impact parameter (i.e. peripheral collision) a magnetic field is created by the positively charged ions moving at almost the speed of the light. Let us evaluate how large magnetic field is expected in the collision at the RHIC energy in a classical manner. For simplicity we assume that the (positively charged) heavy ions are point charges [129]. The collision geometry is schematically modelled as in the left of figure 10. Then, from the Liénard-Wiechert potential, the magnetic fields at the origin reads

$$e\mathbf{B}(\mathbf{x}, t) = \frac{Ze^2}{4\pi} \cdot \frac{b\beta(1-\beta^2)\mathbf{e}_y}{[(\beta t)^2 + (1-\beta^2)(b/2)^2]^{3/2}} = eB_0 \frac{\mathbf{e}_y}{[1 + (t/t_0)^2]^{3/2}}, \quad (54)$$

$$eB_0 = \frac{8Z\alpha_e}{b^2} \sinh(Y) = (47.6 \text{ MeV})^2 \left(\frac{1\text{fm}}{b}\right)^2 Z \sinh(Y),$$

$$t_0 = \frac{b}{2 \sinh(Y)}.$$

In the definition of  $B_0$  and  $t_0$  we use the beam rapidity  $Y$  instead of the velocity  $\beta$ , which is related by  $\beta = \tanh(Y)$ . Here,  $B_0$  is the maximum strength of the magnetic field and  $t_0$  gives a typical time scale of decaying field. In the case of Au-Au collision at the RHIC energy, these parameters are

$$Z = 79, \quad \sinh(Y) \simeq \cosh(Y) = \frac{\sqrt{s_{NN}}}{m_N} \simeq 106.6. \quad (55)$$



The point-charge approximation is valid when the collision is far peripheral. So, let us take  $b = 10$  fm [129]. Then, this simple estimate leads to

$$eB_0 \simeq 1.9 \times 10^5 \text{ MeV}^2 = 3.2 \times 10^{19} \text{ gauss} , \quad t_0 \simeq 0.05 \text{ fm}/c . \quad (56)$$

This magnetic field strength is  $10^4$  times larger than the surface magnetic field of the magnetar, and  $10^7$  times larger than that of the ordinary neutron star. Although such a strong field is transient and decays with the time scale  $t_0$ , we note that the decay is not as steep as exponential damp but power-law suppression. At  $t/t_0 \sim 2 \sim 0.1 \text{ fm}/c$ , for example, the magnetic field diminishes to a tenth of  $B_0$ . We note that this time scale is of order of  $Q_s^{-1}$  where  $Q_s$  is the saturation scale at RHIC [130, 131, 132]. Although there are a number of theoretical calculations of equilibrated QCD matter under strong  $\mathbf{B}$  fields, any serious simulation of the Glasma [133] and the particle production in strong  $\mathbf{B}$  have not been fully analysed. The real-time dynamics of the strong  $\mathbf{B}$  effects needs more investigations.

#### *4.1. Topological properties probed by the magnetic field*

It is well-known that special gauge configurations with non-zero winding number play an important role in understanding of the vacuum structure in the strong interactions. The spontaneous breaking of chiral symmetry is attributed to the QCD instanton which is the origin of dynamical mass generation [134]. The confinement nature is also explained in terms of magnetic monopole condensation in a special class of the gauge choice (see [135] for a lecture note).

There is no doubt about the existence of topological configurations in QCD physics, but it is quite challenging how to “see” such topological contents in real experiments. The Chiral Magnetic Effect (CME) is one of the promising candidates [106, 136, 137]. Let us imagine the following situation specifically; the QCD vacuum accommodates one instanton that has a topological charge  $Q_W$  and a magnetic field  $\mathbf{B}$  that is as strong as the QCD energy scale  $\Lambda_{\text{QCD}}$  is applied on the instanton.

Then, the axial anomaly relation (for the single-flavour case),

$$\partial_\mu j_5^\mu = -\frac{g^2}{8\pi^2} \int d^3x \text{tr} F_{\mu\nu} \tilde{F}^{\mu\nu} , \quad (57)$$

implies that

$$\Delta N_5 = N_5(t = \infty) - N_5(t = -\infty) = -2Q_W . \quad (58)$$

This means that, if the system starts with the chirally neutral situation ( $N_5(t = -\infty) = 0$ ), a finite amount of chirality in the final state is generated by the topological charge during the time evolution. In the chiral limit the momentum and the spin are parallel to each other if the chirality is right-handed, while they are anti-parallel if the chirality is left-handed. The spin is aligned by strong  $\mathbf{B}$ , which makes the momentum also aligned along the  $\mathbf{B}$  direction, leading to a non-vanishing value of the total momentum if  $\Delta N_5 \neq 0$ . In other words, since Dirac fermions are charged, an electric or baryonic current is produced for  $\mathbf{B} \neq 0$  and  $\Delta N_5 \neq 0$ .

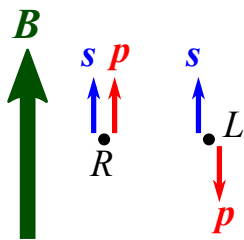


**Figure 11.** Chiral Magnetic Effect: In strong  $\mathbf{B}$  field right-handed particles move in parallel with  $\mathbf{B}$  and left-handed particles in anti-parallel to  $\mathbf{B}$ . A non-zero net flow results from  $N_5 \neq 0$ .

Such an effect can be expressed simply as [136]

$$\mathbf{J}_V = -2Q_W \frac{\mathbf{B}}{|\mathbf{B}|}, \quad (59)$$

for large enough  $\mathbf{B}$ , where  $\mathbf{J}_V$  represents the vector current  $\langle \bar{\psi} \gamma^\mu \psi \rangle$  integrated over the spatial volume.

For arbitrary strength of  $\mathbf{B}$  it is more appropriate to work in the grand canonical ensemble using the chiral chemical potential  $\mu_5$  instead of  $N_5$ . One can then prove non-perturbatively that [106, 138, 139]

$$\mathbf{j}_V = \frac{e\mu_5}{2\pi^2} \mathbf{B} \quad (60)$$

holds for any  $\mathbf{B}$  and  $\mu_5$ . It is easy to confirm that equation (60) is reduced to equation (59) in the strong  $\mathbf{B}$  limit using the anomaly relation (58).

In fact this is one example of more generic relation,

$$\mathbf{j}^\mu = C \varepsilon^{\mu\nu\rho\sigma} \partial_\nu \phi F_{\rho\sigma}. \quad (61)$$

Here  $\phi$  is some field, and in the context of the CME, the strong  $\theta$ -angle is identified as  $\phi$  in the above. Then,  $\nu = 0$ ,  $\rho = x$  and  $\sigma = y$  uniquely fix  $\nu = z$  from  $\varepsilon^{\mu\nu\rho\sigma}$ . By regarding  $\partial_0 \theta$  as  $\mu_5$  [106], one can readily retrieve equation (60) apart from the overall constant. One can also understand related effects from equation (61). If  $\theta$  (or  $\phi$  in the above) is spatially inhomogeneous,  $\nu = z$  (instead of  $\nu = 0$ ) leads to  $\mu = 0$  (instead of  $\mu = 3$ ), meaning that an electric charge or an electric dipole moment is induced [140]. In addition, one can even think of not the  $\theta$ -angle but the pion field  $\pi$  as  $\phi$  in equation (61), and then the presence of time-dependent background, i.e.  $\partial_0 \pi^0$ , results in an effect similar to the CME-induced current. It is actually argued in the Skyrminion model that an additional electric charge is induced in the baryon content (that is constructed as a profile of  $\pi^a(\mathbf{x})$ ) under a strong  $\mathbf{B}$  field [141].

What is detectable in experiments should not be the current  $\mathbf{j}_V$  itself because the QCD vacuum has fluctuations of instantons and anti-instantons. In other words, the parity ( $\mathcal{P}$ ) and the charge-parity ( $\mathcal{CP}$ ) symmetries are broken only (spatially and temporally) locally at the topological excitation, but those symmetries are restored on average over fluctuations. Thus, the CME-induced current  $\mathbf{j}_V$  is also a local object and

the (ensemble or spatial) average makes it vanishing. In this way the CME is one of the candidates to give an account for the “Local Parity Violation” (LPV), if any, that might be observed in the relativistic heavy-ion collisions.

The most relevant quantity to experimental data [142] is fluctuation of the CME-induced current, that is, the electric-current susceptibility  $\chi_j$  [143]. The one-loop result in the small-frequency limit at zero momentum is

$$\chi_j = \frac{e^2 |eB|}{2\pi^2}, \quad (62)$$

which does not depend on  $\mu_5$  and comes from the Landau zero-mode alone, interestingly. There is an intuitive argument to take a short-cut for the derivation of the above expression [143]. For this purpose let us consider the electric-current generation rate,

$$\frac{d(eJ_V)}{dt} = V \frac{e^2 |eB| E}{2\pi^2}, \quad (63)$$

which originates from the correspondence between the chirality generation and the particle production when fields are strong enough [144]. The same quantity can be expressed in the framework of the linear response theory as

$$\begin{aligned} \frac{d(eJ_V)}{dt} &= - \int d^3x d^4x' \left\langle \frac{d(ej_V)(x)}{dt} j_V(x') \right\rangle eA(x') \\ &= \int d^3x d^4x' e^2 \langle j_V(x) j_V(x') \rangle E, \end{aligned} \quad (64)$$

where  $A(x)$  denotes a vector potential component parallel to  $\mathbf{B}$  and  $\mathbf{J}_V$ . From the first line to the second line above, we used  $E = \partial_0 A$ . By equating these (63) and (64), we can immediately find  $\chi_j$  given by equation (62).

#### *4.2. Implication to and from the QCD phase transitions*

Once the CME is confirmed in the heavy-ion collision experiment, it would signal chiral symmetry restoration. This is because, as we have seen in the previous subsection, the CME requires massless Dirac fermions and thus vanishing chiral condensate. It is not obvious what the CME can imply for deconfinement. Generally speaking, the sphaleron transition rate is proportional to  $T^4$  by dimensional reason and real-time topological excitations become abundant at higher temperature [145, 146, 147]. In this argument, however, any feature inherent to deconfined gluons and quarks is not quite needed for the manifestation of the CME. In a solvable model in (1+1) dimensions, as we will discuss later in fact, the CME exists even though no deconfinement takes place.

In the computation of the electric-current susceptibility there is a significant influence from the chiral phase transition. Actually, at finite  $\mu_5$ , the divergent chiral susceptibility has a mixing with the current susceptibility  $\chi_j$  causing enhancement in  $\chi_j$  at the chiral phase transition [148]. It is not yet understood how the Polyakov loop dynamics and the deconfinement transition should affect  $\chi_j$  and any other observable sensitive to the CME.

In principle the lattice-QCD simulation in a strong  $\mathbf{B}$  field can clarify the effect of chiral restoration and deconfinement [107, 108, 149, 150]. There are also some effective model studies on the phase diagram modified by  $\mathbf{B}$  and also the effects of the strong  $\theta$ -angle as well as  $\partial_0\theta$  [151, 152, 153]. It is known by now that the PNJL and PQM model calculations with large  $\mathbf{B}$  are not consistent with the lattice-QCD results in which chiral restoration and deconfinement are locked together for any  $\mathbf{B}$  [154]. This inconsistency could perhaps arise from the missing diagram as shown in figure 9 and the coupling to  $\mathbf{B}$  in the Polyakov loop potential. Besides, the chiral model part may have a non-trivial dependence on the Polyakov loop through the fermionic interaction terms [155, 156].

A careful comparison between results from the effective model approach and from the lattice-QCD simulation at large  $\mathbf{B}$  should be very useful for the finite-density study on QCD matter. In the case at  $\mu_q > T$  it is difficult to impose any reliable constraint from the lattice-QCD simulation, while the finite- $\mathbf{B}$  simulation has no principle problem and one can check quantitatively if the effective model description is valid or inadequate. If it is insufficient to reproduce the lattice data at large  $\mathbf{B}$ , it is most unlikely that the model can encompass the finite-density property of QCD matter either.

One might have thought that the perturbative calculation of the Weiss potential (12) can be extended to the finite- $\mathbf{B}$  case. It is just straightforward to generalise the quark one-loop contribution (18) to the finite- $\mathbf{B}$  calculation. What is more difficult is the polarisation effect as in figure 9. This has been evaluated in the Lowest Landau-Level (LLL) approximation that will be explained in the next subsection for a quick derivation of the CME-induced current and susceptibility. In short summary, the polarisation effect on the Weiss potential has the following effect: The Weiss potential (12) comes from the integration with respect to two transverse gluons, which are physical degrees of freedom and unphysical longitudinal and ghost modes cancel out. In the LLL approximation one can show that only one of two transverse gluons acquires a screening mass proportional to  $\sqrt{eB}$ . The height of the potential decreases up to a half of the original Weiss potential, therefore, with increasing  $\mathbf{B}$ . Qualitatively, a larger  $\mathbf{B}$  tends to reduce the barrier at the confined state with  $\Phi = 0$  and to delay the deconfinement phase transition.

### 4.3. Dimensional reduction

Under a strong magnetic field, in general, the transverse motion of charged particles is equivalent to the one in the harmonic oscillator. The energy level is then discrete due to the Landau quantisation. Spin-1/2 particles have the Landau zero-mode which would dominate in the dynamics at energies below the scale  $\sim \sqrt{eB}$ . Such a strong  $\mathbf{B}$  enables us to use the LLL approximation and to drop the transverse motion at all. In this limit we can reduce the (3+1)-dimensional theory into a form of the (1+1)-dimensional one multiplied by the Landau level density.

In Minkowskian space-time we use the metric  $g^{00} = -g^{11} = 1$ ,  $g^{01} = g^{10} = 0$  and the  $2 \times 2$   $\gamma$ -matrices which satisfy  $\{\gamma^\mu, \gamma^\nu\} = 2g^{\mu\nu}$ . Chirality is characterised by

$\gamma^5 = \gamma^0\gamma^1 = \text{diag}(1, -1)$  in the chiral (Weyl) representation. Therefore the upper (lower) element of two-component spinor  $\psi = (\psi_R, \psi_L)^t$  represents the right-handed (left-handed) particle. In (1+1) dimensions the particle–anti-particle difference is correlated with the chirality. That is, in momentum space, the right-handed component corresponds to a right-moving ( $p > 0$ ) particle and a left-moving ( $p < 0$ ) anti-particle. One can understand the left-handed component in the same way, i.e. a left-moving ( $p < 0$ ) particle and a right-moving ( $p > 0$ ) anti-particle.

In (1+1) dimensions the following relation among the  $\gamma$ -matrices plays an interesting role for the topological currents;

$$\gamma^\mu\gamma^5 = -\varepsilon^{\mu\nu}\gamma_\nu, \quad (65)$$

where  $\varepsilon^{01} = -\varepsilon^{10} = -\varepsilon_{01} = \varepsilon_{10} = 1$ , which relates the vector and the axial-vector currents. As usual, we can write the vector and the axial-vector currents as

$$j_V^\mu = \bar{\psi}\gamma^\mu\psi, \quad j_5^\mu = \bar{\psi}\gamma^\mu\gamma^5\psi. \quad (66)$$

Using the relation (65), we have a relation,  $j_5^\mu = -\varepsilon^{\mu\nu}j_\nu$ , that is explicitly written as [157]

$$j_V^1 = j_5^0, \quad j_5^1 = j_V^0. \quad (67)$$

*4.3.1. Topological currents in (1+1) dimensions:* The relation between the vector and axial-vector currents is very useful because, as we will see here, it captures the essential feature of the CME-induced currents in (3+1) dimensions.

Let us consider the anomaly relation in (1+1) dimensions. It is well-known that the axial anomaly leads to

$$\partial_\mu j_5^\mu = \frac{e}{2\pi}\varepsilon^{\mu\nu}F_{\mu\nu} = \frac{e}{\pi}E = -2q_W, \quad (68)$$

where the electric field is  $E = F^{10}$  in the standard convention. Note that there is no magnetic field but only the electric field  $E$  in (1+1) dimensions. We here defined the (1+1)-dimensional topological charge density as  $q_W = -(e/2\pi)E$  in accord to the convention. By integrating equation (68) over space-time and assuming that the current falls sufficiently fast at spatial infinity, one can recover equation (58) easily. We can also prove that the topological charge,  $Q_W = \int d^2x q_W(x)$ , takes an integer number so that the boundary condition in the  $x$ -direction can be maintained.

We also note that one can express equation (68) in the following form;

$$\partial_\mu j_5^\mu(x) = -\frac{e}{\pi}(\partial^0 A^1 - \partial^1 A^0) = -2\partial_\mu K^\mu(x) \quad (69)$$

with the (1+1)-dimensional Chern-Simons current density defined by  $K^\mu = -(e/2\pi)\varepsilon^{\mu\nu}A_\nu$ . From this identification, the Chern-Simons number in this system is inferred as

$$\nu(t) = \int dx K^0(t, x) = \frac{e}{2\pi} \int dx A^1(t, x). \quad (70)$$

Combining these expressions with the relation  $j_V^1 = j_5^0$  (where  $N_5$  is the volume integral of  $j_5^0$ ), one can immediately write the vector current integrated over space as

$$J_V^1(t) = N_5(t) = -2 \int dt dx q_W(t, x), \quad (71)$$

assuming that  $N_5$  was zero at the initial time ( $N_5(t = -\infty) = 0$ ). This simple relation leads to the current at late time as given by

$$J_V^1 = -2Q_W. \quad (72)$$

This is nothing but the result expected when the spin is fully polarised in the (3+1)-dimensional CME at strong  $\mathbf{B}$  (see equation (59)). Note that in (1+1) dimensions the spin is always fully polarised because there is only one spatial direction and thus the moving direction (either  $p > 0$  or  $p < 0$ ) and the chirality of particles have one-to-one correspondence. Here equation (71) physically means Ohm's law because the (1+1)-dimensional topological charge density is proportional to the electric field as seen in equation (68).

If the spatial component of the Chern-Simons current falls sufficiently fast, the topological charge is written as  $Q_W = \nu(t = \infty) - \nu(t = -\infty)$ . Therefore, (the spatial average of)  $A^1$  is the Chern-Simons number and the boundary condition of  $A^1$  in the  $t$ -direction gives the topological winding number. Supposed that  $\nu(t = -\infty) = N_5(t = -\infty) = 0$ , the topologically induced current is written as

$$J_V^1(t) = -\frac{e}{\pi} \int dx A^1(t, x). \quad (73)$$

If we identify  $-eA^0$  as the chemical potential  $\mu_q$  (regarding the sign, remember the covariant derivative  $p^0 - eA^0$  and the dispersion relation  $p^0 = E_p - \mu_q$  for particles). Equation (65) implies that  $eA^1\gamma^1 = eA^1\gamma^0\gamma^5$  and thus  $-eA^1$  can be regarded as the axial (or chiral) chemical potential  $\mu_5$ . Therefore, one can reach a conclusion that

$$J_V^1 = \frac{1}{\pi} \int dx \mu_5, \quad (74)$$

which correctly recovers the (3+1)-dimensional CME-induced current (60) once one multiply this by the Landau level density,  $eB/(2\pi)$ . That is,

$$\begin{aligned} j_V &= \frac{\mu_5}{\pi} && \text{[in (1+1) dimensions]} \\ \longrightarrow j_V &= \frac{|eB|}{2\pi} \cdot \frac{\mu_5}{\pi}, && \text{[in (3+1) dimensions]} \end{aligned} \quad (75)$$

which coincides with equation (60).

Here, it is clear that the longitudinal gauge field  $A^1$ , which is the Chern-Simons number in (1+1) dimensions, plays the role of the chiral chemical potential  $\mu_5$  in (3+1) dimensions. We note, however, that there is an important difference; usually  $\mu_5$  is introduced by hand as a constant, but in (1+1) dimensions  $A^1$  must have  $t$ -dependence to allow for nonzero  $Q_W$ . We can think of a concrete ‘‘instanton’’ configuration in (1+1) dimensions simply as

$$A^1(t, x) = \frac{2\pi Q_W}{eL} \frac{t}{T} = -Et, \quad (76)$$

where we limit ourselves to the spatially homogeneous case and denote the spatial and temporal extents as  $L$  and  $T$ , respectively, and then we have

$$j_V^1(t) = \frac{J_V^1(t)}{L} = \frac{eE}{\pi}t. \quad (77)$$

From this, again, if multiplied by the Landau-level degeneracy we can correctly recover the current generation rate given by equation (63), i.e.

$$\begin{aligned} \frac{d(ej_V)}{dt} &= \frac{e^2 E}{\pi} && \text{[in (1+1) dimensions]} \\ \longrightarrow \frac{d(ej_V)}{dt} &= \frac{|eB|}{2\pi} \cdot \frac{e^2 E}{\pi}, && \text{[in (3+1) dimensions]} \end{aligned} \quad (78)$$

which coincides with equation (63).

In the same way we can get a finite axial-vector current at finite quark chemical potential  $\mu_q$ . To see the anomalous nature in this case the important fact is that the relation between the density and the chemical potential is given by the quantum anomaly in (1+1) dimensions, that is,

$$n_q = -\frac{eA^0}{\pi}, \quad (79)$$

which results from the (1+1)-dimensional anomaly. One can derive this expression directly from  $n = \langle \psi^\dagger(x)\psi(x) \rangle$  by inserting the gauge field as a regulator as  $\lim_{y^0 \rightarrow x^0} \psi^\dagger(y) \exp[-ie \int dt A^0] \psi(x)$ . From this one can immediately find,

$$J_5^1 = \int dx n_q = \frac{1}{\pi} \int dx \mu_q, \quad (80)$$

which represents the Chiral Separation Effect [140]. This is again the anomaly relation exactly same as that in (3+1) dimensions once multiplied by the Landau level density  $eB/2\pi$ .

*4.3.2. Chiral Magnetic Effect in the Schwinger model:* So far the arguments and the resulting expressions are quite general. From now on we shall go into the dynamical properties calculating microscopic quantities in a solvable (1+1)-dimensional model, i.e. the massless Schwinger model. The easiest way to accomplish a calculation in the Schwinger model is to use the mapping onto a free bosonic theory. In our case, however, the bosonisation rule is a bit more complicated than usual because we deal with not only fermionic fields (such as the chiral condensate) but also gauge fields (such as the electric field). So, the Lagrangian density of the corresponding theory should be

$$\mathcal{L} = \frac{1}{2}(\partial^\mu \theta)(\partial_\mu \theta) - m_\gamma(\partial^\mu \theta)(\partial_\mu \phi) - \frac{1}{2}(\partial^\mu \phi)\partial^2(\partial_\mu \phi) \quad (81)$$

with the boson mass [158],

$$m_\gamma^2 = \frac{e^2}{\pi}. \quad (82)$$

After integrating the  $\phi$ -field out, we get a theory only in terms of the  $\theta$ -field that is free (no interaction term) and has a mass  $m_\gamma$ . Such a scalar theory is usually used with the bosonisation rule [159],

$$j_V^\mu = \bar{\psi}\gamma^\mu\psi = \frac{1}{\sqrt{\pi}}\varepsilon^{\mu\nu}\partial_\nu\theta, \quad (83)$$

$$j_5^\mu = \bar{\psi}\gamma^\mu\gamma^5\psi = -\frac{1}{\sqrt{\pi}}\partial^\mu\theta, \quad (84)$$

$$\bar{\psi}\psi = -cm_\gamma : \cos(2\sqrt{\pi}\theta) : \quad (85)$$

with the normal ordering :. Now we remark that  $\phi$  in the Lagrangian density (81) comes from the gauge field,  $A^\mu = -\varepsilon^{\mu\nu}\partial_\nu\phi$  (where  $\phi$  includes an instanton-like configuration  $\sim \frac{1}{2}Et^2$  which does not satisfy the periodic boundary condition in the  $t$ -direction). Then the electric field takes a form  $E = \partial^2\phi$ . Once we integrate the  $\theta$ -field out from the theory, after the Gaussian integration in the functional formalism, equation (84) is replaced by

$$j_5^\mu = -\frac{1}{\sqrt{\pi}}\partial^\mu\theta \rightarrow -\frac{m_\gamma}{\sqrt{\pi}}\partial^\mu\phi = -\frac{e}{\pi}\partial^\mu\phi. \quad (86)$$

The anomaly relation is then derived as

$$\partial_\mu j_5^\mu = -\frac{e}{\pi}\partial^2\phi = -\frac{e}{\pi}E = -2q_W, \quad (87)$$

which is fully consistent with the anomaly relation (68).

In the same manner we can express the vector current in terms of  $\phi$  to find,

$$j_V^\mu = \frac{e}{\pi}\varepsilon^{\mu\nu}\partial_\nu\phi = 2\varepsilon^{\mu\nu}\frac{\partial_\nu}{\partial^2}q_W. \quad (88)$$

It is easy to make sure that this result is fully consistent with the previous relation again. That is, after the spatial integration on  $\phi$  and  $q_W$  in the above, the spatial derivative  $\partial_1$  drops off and the right-hand side simplifies as  $-2/\partial_0$  for  $\mu = 1$  component, that is just the  $t$ -integration. Therefore the right-hand side finally becomes  $-2Q_W$  together with the spatial integration, and hence we obtain  $J_V^1 = -2Q_W$ .

The above equation gives a microscopic structure of the current in more general cases with spatial modulation. In momentum space we can re-express this as follows;

$$j_V^1(\omega, k) = \frac{-2i\omega}{\omega^2 - k^2} q_W(\omega, k). \quad (89)$$

This is an interesting relation. If  $\omega \rightarrow 0$  is taken first, we see that  $j_V^1(0, k)$  is vanishing. To get the CME-induced current and the non-zero chiral magnetic conductivity, it is necessary to take the zero-momentum limit in the order of  $k \rightarrow 0$  first and then  $\omega \rightarrow 0$  later. This observation is in fact consistent with the result of the one-loop calculation of the conductivity [129].

We point out that the structure of equation (89) naturally appears from the transverse projection. That is, after the one-loop integration with the gauge potential source in momentum space, the well-known result reads;

$$j_V^\mu(\omega, k) = -\left(g^{\mu\nu} - \frac{q^\mu q^\nu}{q^2}\right) \frac{e}{\pi} A_\nu(\omega, k) \quad (90)$$



with  $q = (\omega, k)$  and  $q^2 = \omega^2 - k^2$ , from which one can easily find that

$$j_V^1(\omega, k) = -\frac{\omega^2}{\omega^2 - k^2} \frac{e}{\pi} A^1(\omega, k) . \quad (91)$$

Because  $q_W = (e/\pi)\partial^0 A^1$ , one can substitute  $A^1 = i(2\pi/e)q_W/\omega$  for  $A^1$  above, and one can then check explicitly that the above expression is equivalent to equation (89).

From the equivalence to the bosonised theory it is very easy to read the electric current-current fluctuation too. To this end one should integrate the  $\phi$ -field first, and then what remains is a free massive scalar theory in terms of the  $\theta$ -field alone. Then we trivially get,

$$\chi_j(x - y) = e^2 \langle j^1(x) j^1(y) \rangle = m_\gamma^2 \partial_0^x \partial_0^y \langle \theta(x) \theta(y) \rangle , \quad (92)$$

or in momentum space one can express this as

$$\chi_j(\omega, k) = \frac{m_\gamma^2 \omega^2}{\omega^2 - k^2 - m_\gamma^2 + i\epsilon} . \quad (93)$$

At a first glance this expression looks different from equation (62). This is because the above expression (93) is a result after resummation of the bubble-type diagrams, while equation (62) is the result of the one-loop order. Roughly speaking,  $m_\gamma^2$  appears in the denominator of equation (93) as a result of infinite insertion of the polarisation diagram. This indicates that one can extract the one-loop result from the leading-order Taylor expansion of equation (93) in terms of  $m_\gamma^2$ . That procedure actually leads to

$$\chi_j^{\text{one-loop}}(\omega, k) = \frac{m_\gamma^2 \omega^2}{\omega^2 - k^2} \rightarrow m_\gamma^2 = \frac{e^2}{\pi} \quad (\text{at } k \rightarrow 0) . \quad (94)$$

Therefore,

$$\begin{aligned} \chi_j^{\text{one-loop}} &= \frac{e^2}{\pi} && [\text{in (1+1) dimensions}] \\ \longrightarrow \chi_j^{\text{one-loop}} &= \frac{|eB|}{2\pi} \cdot \frac{e^2}{\pi} , && [\text{in (3+1) dimensions}] \end{aligned} \quad (95)$$

which again coincides with the previous result (62).

In this way the Schwinger model is of great use to understand the topological properties probed by the magnetic field. In reference [160] microscopic calculations to demonstrate how the dimensional reduction occurs in a way consistent with the momentum conservation are given with a more detailed result for the polarisation tensor in (1+1) dimensions embedded in (3+1)-dimensional gauge fields.

## 5. Summary and Outlook

In this review some of the theoretical approaches to QCD matter in extreme environments have been picked up. This direction of physics is strongly motivated by relativistic heavy-ion collision experiments. Furthermore, extreme environments such as the high temperature, the high baryon density and the strong magnetic field would enable theorists to attack QCD problems in a treatable way.

Theoretical and experimental researches on finite- $T$  QCD have achieved the level of the precision science, whereas the finite-density study of QCD is still controversial. Theoretical approaches cannot escape from huge uncertainties, and only the forthcoming experimental data will be able to impose constraints on many possibilities proposed from the theoretical side.

New physics opportunities provided by the strong magnetic field created in the heavy-ion collision are quite intriguing. A deeper understanding in this direction would be helpful for the finite-density study as well. This is because gluons can couple to both the magnetic field effects and the density effects only through the quark polarisation processes.

There are many interesting subjects that we had to miss in this article. Let us look quickly over some of them. We did not discuss the recent developments in the functional RG approach to the QCD phase diagram [161]. This approach is the most promising among others to attack the problem of the QCD phase diagram from the first-principle technique. Future extensions to the three-flavour case without uncertainty that stems from the ( $T$ -dependent) strength of the  $U(1)_A$  anomaly would be desirable if possible. The inhomogeneous chiral condensate (chiral density wave) is the key concept that may reconcile various states of matter in the baryon-rich regime; the QCD critical point, the QCD triple point [162], Quarkyonic Matter and even the dimensionally-reduced state in strong magnetic fields [157]. The relation between the chiral density-wave state and the Polyakov loop dynamics would be a challenging problem too.

Intense magnetic fields have opened a new direction of physics in the heavy-ion collision. The situation realised as a result of the LLL approximation is similar to that near the Fermi surface at high density, i.e. pseudo-(1+1) dimensionality causes peculiar phenomena such as superconductivity [163] and sound modes [164, 165] that may have a connection to the so-called Tomonaga-Luttinger liquid in which no quasi-particle excitations but only sound modes exist.

All these developments and new possibilities are waiting for further investigations.

## Acknowledgments

The author thanks Oleg Andreev, Maxim Chernodub, Gerald Dunne, Eduardo Fraga, Tetsuo Hatsuda, Yoshimasa Hidaka, Dima Kharzeev, Youngman Kim, Toru Kojo, Larry McLerran, Shin Nakamura, Jan Pawłowski, Rob Pisarski, Misha Polikarpov, Marco Ruggieri, Nan Su, Harmen Warringa, Wolfram Weise for useful discussions.

## References

- [1] J. Bjorken, “Highly relativistic nucleus-nucleus collisions: The central rapidity region,” *Phys. Rev.* **D27** (1983) 140–151.
- [2] **Wuppertal-Budapest** Collaboration, S. Borsanyi *et al.*, “Is there still any  $T_c$  mystery in lattice QCD? Results with physical masses in the continuum limit III,” *JHEP* **1009** (2010) 073, [arXiv:1005.3508](https://arxiv.org/abs/1005.3508) [[hep-lat](https://arxiv.org/abs/1005.3508)].

- [3] **HotQCD** Collaboration, A. Bazavov and P. Petreczky, “Chiral transition and deconfinement transition in QCD with the highly improved staggered quark (HISQ) action,” [arXiv:1009.4914 \[hep-lat\]](#).
- [4] I. Vitev, “Jet tomography,” *J. Phys. G* **G30** (2004) S791–S800, [arXiv:hep-ph/0403089 \[hep-ph\]](#).
- [5] M. Asakawa and K. Yazaki, “Chiral restoration at finite density and temperature,” *Nucl. Phys.* **A504** (1989) 668–684.
- [6] A. Barducci, R. Casalbuoni, S. De Curtis, R. Gatto, and G. Pettini, “Chiral symmetry breaking in QCD at finite temperature and density,” *Phys. Lett.* **B231** (1989) 463.
- [7] J. Berges and K. Rajagopal, “Color superconductivity and chiral symmetry restoration at nonzero baryon density and temperature,” *Nucl. Phys.* **B538** (1999) 215–232, [arXiv:hep-ph/9804233](#).
- [8] M. A. Stephanov, K. Rajagopal, and E. V. Shuryak, “Signatures of the tricritical point in QCD,” *Phys. Rev. Lett.* **81** (1998) 4816–4819, [arXiv:hep-ph/9806219](#).
- [9] M. A. Stephanov, K. Rajagopal, and E. V. Shuryak, “Event-by-event fluctuations in heavy ion collisions and the QCD critical point,” *Phys. Rev.* **D60** (1999) 114028, [arXiv:hep-ph/9903292](#).
- [10] K. Fukushima, “Chiral symmetry and heavy-ion collisions,” *J. Phys. G* **G35** (2008) 104020, [arXiv:0806.0292 \[hep-ph\]](#).
- [11] K. Fukushima and T. Hatsuda, “The phase diagram of dense QCD,” *Rept. Prog. Phys.* **74** (2011) 014001, [arXiv:1005.4814 \[hep-ph\]](#).
- [12] D. J. Gross, R. D. Pisarski, and L. G. Yaffe, “QCD and instantons at finite temperature,” *Rev. Mod. Phys.* **53** (1981) 43.
- [13] B. Svetitsky, “Symmetry aspects of finite temperature confinement transitions,” *Phys. Rept.* **132** (1986) 1–53.
- [14] S. P. Klevansky, “The Nambu-Jona-Lasinio model of quantum chromodynamics,” *Rev. Mod. Phys.* **64** (1992) 649–708.
- [15] T. Hatsuda and T. Kunihiro, “QCD phenomenology based on a chiral effective Lagrangian,” *Phys. Rept.* **247** (1994) 221–367, [arXiv:hep-ph/9401310](#).
- [16] H. Meyer-Ortmanns, “Phase transitions in quantum chromodynamics,” *Rev. Mod. Phys.* **68** (1996) 473–598, [arXiv:hep-lat/9608098](#).
- [17] A. V. Smilga, “Physics of thermal QCD,” *Phys. Rept.* **291** (1997) 1–106, [arXiv:hep-ph/9612347](#).
- [18] D. H. Rischke, “The quark-gluon plasma in equilibrium,” *Prog. Part. Nucl. Phys.* **52** (2004) 197–296, [arXiv:nucl-th/0305030](#).
- [19] **Particle Data Group** Collaboration, K. Nakamura *et al.*, “Review of particle physics,” *J. Phys. G* **G37** (2010) 075021.
- [20] J. O. Andersen, E. Braaten, E. Petitgirard, and M. Strickland, “HTL perturbation theory to two loops,” *Phys. Rev.* **D66** (2002) 085016, [arXiv:hep-ph/0205085 \[hep-ph\]](#).
- [21] J. O. Andersen and M. Strickland, “Resummation in hot field theories,” *Annals Phys.* **317** (2005) 281–353, [arXiv:hep-ph/0404164 \[hep-ph\]](#).
- [22] A. M. Polyakov, “Thermal properties of gauge fields and quark liberation,” *Phys. Lett.* **B72** (1978) 477–480.
- [23] L. Susskind, “Lattice models of quark confinement at high temperature,” *Phys. Rev.* **D20** (1979) 2610–2618.
- [24] K. G. Wilson, “Confinement of quarks,” *Phys. Rev.* **D10** (1974) 2445–2459.
- [25] N. Weiss, “The effective potential for the order parameter of gauge theories at finite temperature,” *Phys. Rev.* **D24** (1981) 475.
- [26] N. Weiss, “The Wilson line in finite temperature gauge theories,” *Phys. Rev.* **D25** (1982) 2667.
- [27] V. Belyaev, “Higher loop contributions to effective potential of gauge theory at high temperature,” *Phys. Lett.* **B241** (1990) 91.

- [28] K. Enqvist and K. Kajantie, “Hot gluon matter in a constant  $A_0$  background,” *Z. Phys.* **C47** (1990) 291–296.
- [29] V. Belyaev, “Order parameter and effective potential,” *Phys. Lett.* **B254** (1991) 153–157.
- [30] C. Korthals Altes, “Constrained effective potential in hot QCD,” *Nucl. Phys.* **B420** (1994) 637–668, [arXiv:hep-th/9310195 \[hep-th\]](#).
- [31] V. M. Belyaev, I. I. Kogan, G. W. Semenoff, and N. Weiss, “ $Z(N)$  domains in gauge theories with fermions at high temperature,” *Phys. Lett.* **B277** (1992) 331–336.
- [32] T. Bhattacharya, A. Gocksch, C. Korthals Altes, and R. D. Pisarski, “Interface tension in an  $SU(N)$  gauge theory at high temperature,” *Phys. Rev. Lett.* **66** (1991) 998–1000.
- [33] T. Bhattacharya, A. Gocksch, C. Korthals Altes, and R. D. Pisarski, “ $Z(N)$  interface tension in a hot  $SU(N)$  gauge theory,” *Nucl. Phys.* **B383** (1992) 497–524, [arXiv:hep-ph/9205231 \[hep-ph\]](#).
- [34] C. Korthals-Altes, A. Kovner, and M. A. Stephanov, “Spatial ’t Hooft loop, hot QCD and  $Z(N)$  domain walls,” *Phys. Lett.* **B469** (1999) 205–212, [arXiv:hep-ph/9909516 \[hep-ph\]](#).
- [35] G. ’t Hooft, “On the phase transition towards permanent quark confinement,” *Nucl. Phys.* **B138** (1978) 1.
- [36] H. Reinhardt, “On ’t Hooft’s loop operator,” *Phys. Lett.* **B557** (2003) 317–323, [arXiv:hep-th/0212264 \[hep-th\]](#).
- [37] P. de Forcrand and D. Noth, “Precision lattice calculation of  $SU(2)$  ’t Hooft loops,” *Phys. Rev.* **D72** (2005) 114501, [arXiv:hep-lat/0506005 \[hep-lat\]](#).
- [38] K. Fukushima and K. Ohta, “Stability of the perturbative vacuum against spatial variations of the Polyakov loop,” *J. Phys. G* **G26** (2000) 1397–1415, [arXiv:hep-ph/0011108 \[hep-ph\]](#).
- [39] E. Braaten, “Solution to the perturbative infrared catastrophe of hot gauge theories,” *Phys. Rev. Lett.* **74** (1995) 2164–2167, [arXiv:hep-ph/9409434 \[hep-ph\]](#).
- [40] T. Appelquist and R. D. Pisarski, “High-temperature Yang-Mills theories and three-dimensional quantum chromodynamics,” *Phys. Rev.* **D23** (1981) 2305.
- [41] E. Braaten and A. Nieto, “Free energy of QCD at high temperature,” *Phys. Rev.* **D53** (1996) 3421–3437, [arXiv:hep-ph/9510408 \[hep-ph\]](#).
- [42] M. Laine and Y. Schroder, “Two-loop QCD gauge coupling at high temperatures,” *JHEP* **0503** (2005) 067, [arXiv:hep-ph/0503061 \[hep-ph\]](#).
- [43] J. Moller and Y. Schroder, “Open problems in hot QCD,” *Nucl. Phys. Proc. Suppl.* **205–206** (2010) 218–223, [arXiv:1007.1223 \[hep-ph\]](#).
- [44] F. Karsch, E. Laermann, and M. Lutgemeier, “Three-dimensional  $SU(3)$  gauge theory and the spatial string tension of the  $(3+1)$ -dimensional finite temperature  $SU(3)$  gauge theory,” *Phys. Lett.* **B346** (1995) 94–98, [arXiv:hep-lat/9411020 \[hep-lat\]](#).
- [45] M. J. Teper, “ $SU(N)$  gauge theories in  $(2+1)$ -dimensions,” *Phys. Rev.* **D59** (1999) 014512, [arXiv:hep-lat/9804008 \[hep-lat\]](#).
- [46] B. Lucini and M. Teper, “ $SU(N)$  gauge theories in  $(2+1)$ -dimensions: Further results,” *Phys. Rev.* **D66** (2002) 097502, [arXiv:hep-lat/0206027 \[hep-lat\]](#).
- [47] Y. Hidaka and R. D. Pisarski, “Hard thermal loops, to quadratic order, in the background of a spatial ’t Hooft loop,” *Phys. Rev.* **D80** (2009) 036004, [arXiv:0906.1751 \[hep-ph\]](#).
- [48] C. DeTar and U. Heller, “QCD thermodynamics from the lattice,” *Eur. Phys. J.* **A41** (2009) 405–437, [arXiv:0905.2949 \[hep-lat\]](#).
- [49] J. Polonyi and K. Szlachanyi, “Phase transition from strong coupling expansion,” *Phys. Lett.* **B110** (1982) 395–398.
- [50] M. Gross, J. Bartholomew, and D. Hochberg, “ $SU(N)$  deconfinement transition and the  $N$  state clock model,”
- [51] J. B. Kogut, M. Snow, and M. Stone, “Mean field and Monte Carlo studies of  $SU(N)$  chiral models in three-dimensions,” *Nucl. Phys.* **B200** (1982) 211.
- [52] E.-M. Ilgenfritz and J. Kripfganz, “Dynamical fermions at nonzero chemical potential and temperature: mean field approach,” *Z. Phys.* **C29** (1985) 79–82.

- [53] A. Gocksch and M. Ogilvie, “Finite temperature deconfinement and chiral symmetry restoration at strong coupling,” *Phys. Rev.* **D31** (1985) 877.
- [54] K. Fukushima, “Effects of chiral restoration on the behavior of the Polyakov loop at strong coupling,” *Phys. Lett.* **B553** (2003) 38–44, [arXiv:hep-ph/0209311 \[hep-ph\]](#).
- [55] K. Fukushima, “Relation between the Polyakov loop and the chiral order parameter at strong coupling,” *Phys. Rev.* **D68** (2003) 045004, [arXiv:hep-ph/0303225 \[hep-ph\]](#).
- [56] A. Gocksch and R. D. Pisarski, “Partition function for the eigenvalues of the Wilson line,” *Nucl. Phys.* **B402** (1993) 657–668, [arXiv:hep-ph/9302233 \[hep-ph\]](#).
- [57] F. Lenz and M. Thies, “Polyakov loop dynamics in the center symmetric phase,” *Annals Phys.* **268** (1998) 308–358, [arXiv:hep-th/9802066 \[hep-th\]](#).
- [58] K. Fukushima, “Toward understanding the lattice QCD results from the strong coupling analysis,” *Prog. Theor. Phys. Suppl.* **153** (2004) 204–219, [arXiv:hep-ph/0312057 \[hep-ph\]](#).
- [59] S. Roessner, C. Ratti, and W. Weise, “Polyakov loop, diquarks and the two-flavour phase diagram,” *Phys. Rev.* **D75** (2007) 034007, [arXiv:hep-ph/0609281 \[hep-ph\]](#).
- [60] S. Gupta, K. Huebner, and O. Kaczmarek, “Renormalized Polyakov loops in many representations,” *Phys. Rev.* **D77** (2008) 034503, [arXiv:0711.2251 \[hep-lat\]](#).
- [61] K. Fukushima, “QCD thermodynamics and the Polyakov loop,” *Acta Phys. Polon. Supp.* **3** (2010) 567–576.
- [62] A. M. Polyakov, “Gauge fields as rings of glue,” *Nucl. Phys.* **B164** (1980) 171–188.
- [63] M. Creutz, “Monte Carlo study of renormalization in lattice gauge theory,” *Phys. Rev.* **D23** (1981) 1815.
- [64] O. Kaczmarek, F. Karsch, P. Petreczky, and F. Zantow, “Heavy quark anti-quark free energy and the renormalized Polyakov loop,” *Phys. Lett.* **B543** (2002) 41–47, [arXiv:hep-lat/0207002 \[hep-lat\]](#).
- [65] A. Dumitru, Y. Hatta, J. Lenaghan, K. Orginos, and R. D. Pisarski, “Deconfining phase transition as a matrix model of renormalized Polyakov loops,” *Phys. Rev.* **D70** (2004) 034511, [arXiv:hep-th/0311223 \[hep-th\]](#).
- [66] G. ’t Hooft, “A planar diagram theory for strong interactions,” *Nucl. Phys.* **B72** (1974) 461.
- [67] E. Witten, “Baryons in the  $1/n$  expansion,” *Nucl. Phys.* **B160** (1979) 57.
- [68] A. Dumitru, J. Lenaghan, and R. D. Pisarski, “Deconfinement in matrix models about the Gross-Witten point,” *Phys. Rev.* **D71** (2005) 074004, [arXiv:hep-ph/0410294](#).
- [69] E. Witten, “Anti-de Sitter space, thermal phase transition, and confinement in gauge theories,” *Adv. Theor. Math. Phys.* **2** (1998) 505–532, [arXiv:hep-th/9803131 \[hep-th\]](#).
- [70] I. R. Klebanov, “TASI lectures: Introduction to the AdS / CFT correspondence,” [arXiv:hep-th/0009139 \[hep-th\]](#).
- [71] U. Gursoy, E. Kiritsis, L. Mazzanti, and F. Nitti, “Deconfinement and gluon plasma dynamics in improved holographic QCD,” *Phys. Rev. Lett.* **101** (2008) 181601, [arXiv:0804.0899 \[hep-th\]](#).
- [72] S. S. Gubser and A. Nellore, “Mimicking the QCD equation of state with a dual black hole,” *Phys. Rev.* **D78** (2008) 086007, [arXiv:0804.0434 \[hep-th\]](#).
- [73] A. Karch, E. Katz, D. T. Son, and M. A. Stephanov, “Linear confinement and AdS/QCD,” *Phys. Rev.* **D74** (2006) 015005, [arXiv:hep-ph/0602229 \[hep-ph\]](#).
- [74] K. Ghoroku, N. Maru, M. Tachibana, and M. Yahiro, “Holographic model for hadrons in deformed AdS<sub>5</sub> background,” *Phys. Lett.* **B633** (2006) 602–606, [arXiv:hep-ph/0510334 \[hep-ph\]](#).
- [75] O. Andreev and V. I. Zakharov, “The spatial string tension, thermal phase transition, and AdS/QCD,” *Phys. Lett.* **B645** (2007) 437–441, [arXiv:hep-ph/0607026 \[hep-ph\]](#).
- [76] C. P. Herzog, “A holographic prediction of the deconfinement temperature,” *Phys. Rev. Lett.* **98** (2007) 091601, [arXiv:hep-th/0608151 \[hep-th\]](#).
- [77] O. Andreev, “Renormalized Polyakov loop in the deconfined phase of SU( $N$ ) gauge theory and gauge/string duality,” *Phys. Rev. Lett.* **102** (2009) 212001, [arXiv:0903.4375 \[hep-ph\]](#).

- [78] G. Policastro, D. Son, and A. Starinets, “The shear viscosity of strongly coupled  $N=4$  supersymmetric Yang-Mills plasma,” *Phys. Rev. Lett.* **87** (2001) 081601, [arXiv:hep-th/0104066 \[hep-th\]](#).
- [79] P. Kovtun, D. Son, and A. Starinets, “Viscosity in strongly interacting quantum field theories from black hole physics,” *Phys. Rev. Lett.* **94** (2005) 111601, [arXiv:hep-th/0405231 \[hep-th\]](#). An Essay submitted to 2004 Gravity Research Foundation competition.
- [80] A. Jakovac and D. Nogradi, “Shear viscosity of pure Yang-Mills theory at strong coupling,” [arXiv:0810.4181 \[hep-th\]](#).
- [81] N. Itoh, “Hydrostatic equilibrium of hypothetical quark stars,” *Prog. Theor. Phys.* **44** (1970) 291.
- [82] J. C. Collins and M. Perry, “Superdense matter: Neutrons or asymptotically free quarks?,” *Phys. Rev. Lett.* **34** (1975) 1353.
- [83] J. Cleymans, H. Oeschler, K. Redlich, and S. Wheaton, “Comparison of chemical freeze-out criteria in heavy-ion collisions,” *Phys. Rev.* **C73** (2006) 034905, [arXiv:hep-ph/0511094 \[hep-ph\]](#).
- [84] F. Becattini, J. Manninen, and M. Gazdzicki, “Energy and system size dependence of chemical freeze-out in relativistic nuclear collisions,” *Phys. Rev.* **C73** (2006) 044905, [arXiv:hep-ph/0511092 \[hep-ph\]](#).
- [85] A. Andronic, P. Braun-Munzinger, and J. Stachel, “Thermal hadron production in relativistic nuclear collisions: The Hadron mass spectrum, the horn, and the QCD phase transition,” *Phys. Lett.* **B673** (2009) 142–145, [arXiv:0812.1186 \[nucl-th\]](#).
- [86] F. Karsch and K. Redlich, “Probing freeze-out conditions in heavy ion collisions with moments of charge fluctuations,” *Phys. Lett.* **B695** (2011) 136–142, [arXiv:1007.2581 \[hep-ph\]](#).
- [87] P. Braun-Munzinger, J. Stachel, and C. Wetterich, “Chemical freezeout and the QCD phase transition temperature,” *Phys. Lett.* **B596** (2004) 61–69, [arXiv:nucl-th/0311005 \[nucl-th\]](#).
- [88] M. G. Alford, A. Schmitt, K. Rajagopal, and T. Schafer, “Color superconductivity in dense quark matter,” *Rev. Mod. Phys.* **80** (2008) 1455–1515, [arXiv:0709.4635 \[hep-ph\]](#).
- [89] B. A. Freedman and L. D. McLerran, “Fermions and gauge vector mesons at finite temperature and density. 1. Formal techniques,” *Phys. Rev.* **D16** (1977) 1130.
- [90] B. A. Freedman and L. D. McLerran, “Fermions and gauge vector mesons at finite temperature and density. 2. The ground state energy of a relativistic electron gas,” *Phys. Rev.* **D16** (1977) 1147.
- [91] B. A. Freedman and L. D. McLerran, “Fermions and gauge vector mesons at finite temperature and density. 3. The ground state energy of a relativistic quark gas,” *Phys. Rev.* **D16** (1977) 1169.
- [92] C. Korthals Altes, R. D. Pisarski, and A. Sinkovics, “The potential for the phase of the Wilson line at nonzero quark density,” *Phys. Rev.* **D61** (2000) 056007, [arXiv:hep-ph/9904305 \[hep-ph\]](#).
- [93] S. Muroya, A. Nakamura, C. Nonaka, and T. Takaishi, “Lattice QCD at finite density: An introductory review,” *Prog. Theor. Phys.* **110** (2003) 615–668, [arXiv:hep-lat/0306031 \[hep-lat\]](#).
- [94] A. Dumitru, R. D. Pisarski, and D. Zschiesche, “Dense quarks, and the fermion sign problem, in a  $SU(N)$  matrix model,” *Phys. Rev.* **D72** (2005) 065008, [arXiv:hep-ph/0505256 \[hep-ph\]](#).
- [95] K. Fukushima and Y. Hidaka, “A model study of the sign problem in the mean-field approximation,” *Phys. Rev.* **D75** (2007) 036002, [arXiv:hep-ph/0610323 \[hep-ph\]](#).
- [96] S. Nakamura, H. Ooguri, and C.-S. Park, “Gravity dual of spatially modulated phase,” *Phys. Rev.* **D81** (2010) 044018, [arXiv:0911.0679 \[hep-th\]](#).
- [97] S. Nakamura, Y. Seo, S.-J. Sin, and K. Yogendran, “A new phase at finite quark density from AdS/CFT,” *J. Korean Phys. Soc.* **52** (2008) 1734–1739, [arXiv:hep-th/0611021 \[hep-th\]](#).

- [98] Y. Kim, B.-H. Lee, S. Nam, C. Park, and S.-J. Sin, “Deconfinement phase transition in holographic QCD with matter,” *Phys. Rev.* **D76** (2007) 086003, [arXiv:0706.2525 \[hep-ph\]](#).
- [99] K. Jo, B.-H. Lee, C. Park, and S.-J. Sin, “Holographic QCD in medium: A bottom up approach,” *JHEP* **1006** (2010) 022, [arXiv:0909.3914 \[hep-ph\]](#).
- [100] F. Green and F. Karsch, “Mean field analysis of  $SU(N)$  deconfining transitions in the presence of dynamical quarks,” *Nucl. Phys.* **B238** (1984) 297.
- [101] A. Nakamura, “Quarks and gluons at finite temperature and density,” *Phys. Lett.* **B149** (1984) 391.
- [102] J. B. Kogut, M. A. Stephanov, and D. Toublan, “On two-color QCD with baryon chemical potential,” *Phys. Lett.* **B464** (1999) 183–191, [arXiv:hep-ph/9906346](#).
- [103] S. Hands, S. Kim, and J.-I. Skullerud, “Deconfinement in dense 2-color QCD,” *Eur. Phys. J.* **C48** (2006) 193, [arXiv:hep-lat/0604004](#).
- [104] D. T. Son and M. A. Stephanov, “QCD at finite isospin density,” *Phys. Rev. Lett.* **86** (2001) 592–595, [arXiv:hep-ph/0005225](#).
- [105] J. Kogut and D. Sinclair, “Lattice QCD at finite isospin density at zero and finite temperature,” *Phys. Rev.* **D66** (2002) 034505, [arXiv:hep-lat/0202028 \[hep-lat\]](#).
- [106] K. Fukushima, D. E. Kharzeev, and H. J. Warringa, “The chiral magnetic effect,” *Phys. Rev.* **D78** (2008) 074033, [arXiv:0808.3382 \[hep-ph\]](#).
- [107] A. Yamamoto, “Chiral magnetic effect in lattice QCD with a chiral chemical potential,” *Phys. Rev. Lett.* **107** (2011) 031601, [arXiv:1105.0385 \[hep-lat\]](#).
- [108] A. Yamamoto, “Lattice QCD simulation at finite chiral chemical potential,” [arXiv:1108.0937 \[hep-lat\]](#).
- [109] M. G. Alford, A. Kapustin, and F. Wilczek, “Imaginary chemical potential and finite fermion density on the lattice,” *Phys. Rev.* **D59** (1999) 054502, [arXiv:hep-lat/9807039](#).
- [110] P. de Forcrand and O. Philipsen, “The QCD phase diagram for small densities from imaginary chemical potential,” *Nucl. Phys.* **B642** (2002) 290–306, [arXiv:hep-lat/0205016](#).
- [111] M. D’Elia and F. Sanfilippo, “Thermodynamics of two flavor QCD from imaginary chemical potentials,” *Phys. Rev.* **D80** (2009) 014502, [arXiv:0904.1400 \[hep-lat\]](#).
- [112] A. Roberge and N. Weiss, “Gauge theories with imaginary chemical potential and the phases of QCD,” *Nucl. Phys.* **B275** (1986) 734.
- [113] Y. Nishida, “Phase structures of strong coupling lattice QCD with finite baryon and isospin density,” *Phys. Rev.* **D69** (2004) 094501, [arXiv:hep-ph/0312371 \[hep-ph\]](#).
- [114] K. Miura, T. Z. Nakano, A. Ohnishi, and N. Kawamoto, “Phase diagram evolution at finite coupling in strong coupling lattice QCD,” *Phys. Rev.* **D80** (2009) 074034, [arXiv:0907.4245 \[hep-lat\]](#).
- [115] P. de Forcrand and M. Fromm, “Nuclear Physics from lattice QCD at strong coupling,” *Phys. Rev. Lett.* **104** (2010) 112005, [arXiv:0907.1915 \[hep-lat\]](#).
- [116] L. McLerran and R. D. Pisarski, “Phases of cold, dense quarks at large  $N_c$ ,” *Nucl. Phys.* **A796** (2007) 83–100, [arXiv:0706.2191 \[hep-ph\]](#).
- [117] T. Kojo, Y. Hidaka, L. McLerran, and R. D. Pisarski, “Quarkyonic chiral spirals,” *Nucl. Phys.* **A843** (2010) 37–58, [arXiv:0912.3800 \[hep-ph\]](#).
- [118] T. Kojo, Y. Hidaka, K. Fukushima, L. McLerran, and R. D. Pisarski, “Interweaving chiral spirals,” [arXiv:1107.2124 \[hep-ph\]](#).
- [119] K. Fukushima, “Chiral effective model with the Polyakov loop,” *Phys. Lett.* **B591** (2004) 277–284, [arXiv:hep-ph/0310121 \[hep-ph\]](#).
- [120] C. Ratti, M. A. Thaler, and W. Weise, “Phases of QCD: Lattice thermodynamics and a field theoretical model,” *Phys. Rev.* **D73** (2006) 014019, [arXiv:hep-ph/0506234 \[hep-ph\]](#).
- [121] B.-J. Schaefer, J. M. Pawłowski, and J. Wambach, “The phase structure of the Polyakov–Quark–Meson model,” *Phys. Rev.* **D76** (2007) 074023, [arXiv:0704.3234 \[hep-ph\]](#).

- [122] G. Baym and G. Grinstein, “Phase transition in the sigma model at finite temperature,” *Phys. Rev.* **D15** (1977) 2897–2912.
- [123] T. K. Herbst, J. M. Pawłowski, and B.-J. Schaefer, “The phase structure of the Polyakov–quark-meson model beyond mean field,” *Phys. Lett.* **B696** (2011) 58–67, [arXiv:1008.0081 \[hep-ph\]](#).
- [124] V. Skokov, B. Stokic, B. Friman, and K. Redlich, “Meson fluctuations and thermodynamics of the Polyakov loop extended quark-meson model,” *Phys. Rev.* **C82** (2010) 015206, [arXiv:1004.2665 \[hep-ph\]](#).
- [125] A. Dumitru and R. D. Pisarski, “Event-by-event fluctuations from decay of a Polyakov loop condensate,” *Phys. Lett.* **B504** (2001) 282–290, [arXiv:hep-ph/0010083 \[hep-ph\]](#).
- [126] C. Wetterich, “Exact evolution equation for the effective potential,” *Phys. Lett.* **B301** (1993) 90–94.
- [127] K. Fukushima, “Phase diagrams in the three-flavor Nambu–Jona-Lasinio model with the Polyakov loop,” *Phys. Rev.* **D77** (2008) 114028, [arXiv:0803.3318 \[hep-ph\]](#).
- [128] K. Fukushima, “Phase diagram of hot and dense QCD constrained by the Statistical Model,” *Phys. Lett.* **B695** (2011) 387–391, [arXiv:1006.2596 \[hep-ph\]](#).
- [129] D. E. Kharzeev and H. J. Warringa, “Chiral magnetic conductivity,” *Phys. Rev.* **D80** (2009) 034028, [arXiv:0907.5007 \[hep-ph\]](#).
- [130] L. D. McLerran and R. Venugopalan, “Computing quark and gluon distribution functions for very large nuclei,” *Phys. Rev.* **D49** (1994) 2233–2241, [arXiv:hep-ph/9309289 \[hep-ph\]](#).
- [131] L. D. McLerran and R. Venugopalan, “Gluon distribution functions for very large nuclei at small transverse momentum,” *Phys. Rev.* **D49** (1994) 3352–3355, [arXiv:hep-ph/9311205 \[hep-ph\]](#).
- [132] L. D. McLerran and R. Venugopalan, “Green’s functions in the color field of a large nucleus,” *Phys. Rev.* **D50** (1994) 2225–2233, [arXiv:hep-ph/9402335 \[hep-ph\]](#).
- [133] T. Lappi and L. McLerran, “Some features of the glasma,” *Nucl. Phys.* **A772** (2006) 200–212, [arXiv:hep-ph/0602189 \[hep-ph\]](#).
- [134] D. Diakonov, “Chiral symmetry breaking by instantons,” [arXiv:hep-ph/9602375 \[hep-ph\]](#).
- [135] G. ’t Hooft, “Monopoles, instantons and confinement,” [arXiv:hep-th/0010225 \[hep-th\]](#).  
Notes written by Falk Bruckmann, Jena U., Oct 2000.
- [136] D. E. Kharzeev, L. D. McLerran, and H. J. Warringa, “The effects of topological charge change in heavy ion collisions: ‘Event by event P and CP violation’,” *Nucl. Phys.* **A803** (2008) 227–253, [arXiv:0711.0950 \[hep-ph\]](#).
- [137] D. E. Kharzeev, “Topologically induced local P and CP violation in QCD x QED,” *Annals Phys.* **325** (2010) 205–218, [arXiv:0911.3715 \[hep-ph\]](#).
- [138] M. A. Metlitski and A. R. Zhitnitsky, “Anomalous axion interactions and topological currents in dense matter,” *Phys. Rev.* **D72** (2005) 045011, [arXiv:hep-ph/0505072 \[hep-ph\]](#).
- [139] A. Vilenkin, “Equilibrium parity violating current in a magnetic field,” *Phys. Rev.* **D22** (1980) 3080–3084.
- [140] D. Kharzeev and A. Zhitnitsky, “Charge separation induced by P-odd bubbles in QCD matter,” *Nucl. Phys.* **A797** (2007) 67–79, [arXiv:0706.1026 \[hep-ph\]](#).
- [141] M. Eto, K. Hashimoto, H. Iida, T. Ishii, and Y. Maezawa, “Anomaly-induced charges in nucleons,” [arXiv:1103.5443 \[hep-ph\]](#).
- [142] **STAR** Collaboration, B. Abelev *et al.*, “Azimuthal charged-particle correlations and possible local strong parity violation,” *Phys. Rev. Lett.* **103** (2009) 251601, [arXiv:0909.1739 \[nucl-ex\]](#).
- [143] K. Fukushima, D. E. Kharzeev, and H. J. Warringa, “Electric-current susceptibility and the chiral magnetic effect,” *Nucl. Phys.* **A836** (2010) 311–336, [arXiv:0912.2961 \[hep-ph\]](#).
- [144] K. Fukushima, D. E. Kharzeev, and H. J. Warringa, “Real-time dynamics of the Chiral Magnetic Effect,” *Phys. Rev. Lett.* **104** (2010) 212001, [arXiv:1002.2495 \[hep-ph\]](#).
- [145] P. B. Arnold and L. D. McLerran, “The sphaleron strikes back,” *Phys. Rev.* **D37** (1988) 1020.



- [146] L. D. McLerran, E. Mottola, and M. E. Shaposhnikov, “Sphalerons and axion dynamics in high temperature QCD,” *Phys. Rev.* **D43** (1991) 2027–2035.
- [147] D. Bodeker, G. D. Moore, and K. Rummukainen, “Chern-Simons number diffusion and hard thermal loops on the lattice,” *Phys. Rev.* **D61** (2000) 056003, [arXiv:hep-ph/9907545](#) [hep-ph].
- [148] K. Fukushima, M. Ruggieri, and R. Gatto, “Chiral magnetic effect in the PNJL model,” *Phys. Rev.* **D81** (2010) 114031, [arXiv:1003.0047](#) [hep-ph].
- [149] M. Abramczyk, T. Blum, G. Petropoulos, and R. Zhou, “Chiral magnetic effect in 2+1 flavor QCD+QED,” *PoS LAT2009* (2009) 181, [arXiv:0911.1348](#) [hep-lat].
- [150] P. Buividovich, M. Chernodub, E. Luschevskaya, and M. Polikarpov, “Numerical evidence of chiral magnetic effect in lattice gauge theory,” *Phys. Rev.* **D80** (2009) 054503, [arXiv:0907.0494](#) [hep-lat].
- [151] D. Boer and J. K. Boomsma, “Spontaneous CP-violation in the strong interaction at  $\theta = \pi$ ,” *Phys. Rev.* **D78** (2008) 054027, [arXiv:0806.1669](#) [hep-ph].
- [152] J. K. Boomsma and D. Boer, “The High temperature CP-restoring phase transition at  $\theta = \pi$ ,” *Phys. Rev.* **D80** (2009) 034019, [arXiv:0905.4660](#) [hep-ph].
- [153] A. J. Mizher, M. Chernodub, and E. S. Fraga, “Phase diagram of hot QCD in an external magnetic field: possible splitting of deconfinement and chiral transitions,” *Phys. Rev.* **D82** (2010) 105016, [arXiv:1004.2712](#) [hep-ph].
- [154] M. D’Elia, S. Mukherjee, and F. Sanfilippo, “QCD phase transition in a strong magnetic background,” *Phys. Rev.* **D82** (2010) 051501, [arXiv:1005.5365](#) [hep-lat].
- [155] K.-I. Kondo, “Toward a first-principle derivation of confinement and chiral-symmetry-breaking crossover transitions in QCD,” *Phys. Rev.* **D82** (2010) 065024, [arXiv:1005.0314](#) [hep-th].
- [156] R. Gatto and M. Ruggieri, “Deconfinement and chiral symmetry restoration in a strong magnetic background,” *Phys. Rev.* **D83** (2011) 034016, [arXiv:1012.1291](#) [hep-ph].
- [157] G. Basar, G. V. Dunne, and D. E. Kharzeev, “Chiral magnetic spiral,” *Phys. Rev. Lett.* **104** (2010) 232301, [arXiv:1003.3464](#) [hep-ph].
- [158] J. S. Schwinger, “Gauge invariance and mass. 2.,” *Phys. Rev.* **128** (1962) 2425–2429.
- [159] A. V. Smilga, “On the fermion condensate in Schwinger model,” *Phys. Lett.* **B278** (1992) 371–376.
- [160] K. Fukushima, “Magnetic-field induced screening effect and collective excitations,” *Phys. Rev.* **D83** (2011) 111501, [arXiv:1103.4430](#) [hep-ph].
- [161] J. Braun, L. M. Haas, F. Marhauser, and J. M. Pawłowski, “Phase structure of two-flavor QCD at finite chemical potential,” *Phys. Rev. Lett.* **106** (2011) 022002, [arXiv:0908.0008](#) [hep-ph].
- [162] A. Andronic, D. Blaschke, P. Braun-Munzinger, J. Cleymans, K. Fukushima, *et al.*, “Hadron production in ultra-relativistic nuclear collisions: Quarkyonic Matter and a triple point in the phase diagram of QCD,” *Nucl. Phys.* **A837** (2010) 65–86, [arXiv:0911.4806](#) [hep-ph].
- [163] M. Chernodub, “Spontaneous electromagnetic superconductivity of vacuum in strong magnetic field: evidence from the Nambu–Jona-Lasinio model,” *Phys. Rev. Lett.* **106** (2011) 142003, [arXiv:1101.0117](#) [hep-ph].
- [164] D. E. Kharzeev and H.-U. Yee, “Chiral magnetic wave,” *Phys. Rev.* **D83** (2011) 085007, [arXiv:1012.6026](#) [hep-th].
- [165] Y. Burnier, D. E. Kharzeev, J. Liao, and H.-U. Yee, “Chiral magnetic wave at finite baryon density and the electric quadrupole moment of quark-gluon plasma in heavy ion collisions,” *Phys. Rev. Lett.* **107** (2011) 052303, [arXiv:1103.1307](#) [hep-ph].